

**Immobilization of titanium dioxide in crushed recycled glass for atrazine  
photo-degradation**

By

**Amarillys Avilés Miranda**

A thesis submitted in partial fulfillment of the requirements for the degree of

MASTER OF SCIENCE  
In  
CIVIL ENGINEERING  
(Environmental Engineering and Water Resources)

University of Puerto Rico  
Mayagüez Campus

2016

Approved by:

\_\_\_\_\_  
Pedro J. Tarafa Vélez, Ph.D.  
Chairperson, Graduate Committee

\_\_\_\_\_  
Date

\_\_\_\_\_  
O. Marcelo Suárez, Ph.D.  
Co-chair, Graduate Committee

\_\_\_\_\_  
Date

\_\_\_\_\_  
Sangchul Hwang, Ph.D.  
Member, Graduate Committee

\_\_\_\_\_  
Date

\_\_\_\_\_  
Aldo Acevedo Rullán, Ph.D.  
Representative, Graduate School

\_\_\_\_\_  
Date

\_\_\_\_\_  
Prof. Ismael Pagán Trinidad  
Director, Department of Civil Engineering  
and Surveying

\_\_\_\_\_  
Date

## ABSTRACT

The release of toxic chemicals, as herbicides from agricultural activities is causing contamination of surface water by runoffs action after precipitation. This research studied the degradation of atrazine (herbicide) by a porous glass substrate, embedded with photo-catalytic titanium dioxide ( $\text{TiO}_2$ ) nanoparticles. Porous substrate was attained by sintering clear recycled glass cullets (MG-30) in a furnace at temperatures between  $950^\circ\text{C}$  to  $975^\circ\text{C}$  for 45 to 75 minutes. The  $\text{TiO}_2$  nanoparticles were deposited within or onto the glass substrate and immobilized by heat treatment. The polymorph phase of the immobilized  $\text{TiO}_2$  was analyzed after the heat treatment by x-ray diffraction (XRD). Also, a percolation and compressive strength were studied to evaluate the thermo-mechanical properties of the material. The experimental results demonstrated that the  $\text{TiO}_2$  immobilization was favored by sintering nanoparticles within the glass particles, under UV light exposure atrazine degradation capacity was low. On the other hand, the immobilization of the nanoparticles onto the surface increased after the heat treatment. In addition, the XRD analyses confirmed the anatase polymorph phase of the nanoparticles. For the deposition onto the glass substrate, atrazine degradation fell below detection limits after 12 h of UV light exposure with possible exhaustion of the  $\text{TiO}_2$  nanoparticles after 36 h of treatment. Finally, that percolation rate declined for longer sintering time and higher sintering temperature. Conversely, the compressive strength increases for similar sintering parameter changes.

## RESUMEN

La liberación de compuestos tóxicos provenientes de actividades agrícolas como el uso de herbicidas causa contaminación de suministro de agua potable por las escorrentías generadas por la precipitación. Esta investigación estudia la degradación de atrazina, (herbicida), por un sustrato poroso de vidrio funcionalizado con nano-partículas de  $\text{TiO}_2$ . El sustrato fue fabricado por la sinterización de vidrio reciclado triturado entre  $950^\circ\text{C}$  a  $975^\circ\text{C}$  por 45 a 75 min. Las partículas de  $\text{TiO}_2$  fueron depositadas entre o sobre el sustrato de vidrio e inmovilizadas por la exposición a calor. La fase polimórfica del vidrio fue analizada luego de esta exposición térmica por difracción de rayos X. También, análisis de percolación y compresión fueron estudiados para evaluar las propiedades termo-mecánicas del material. Los resultados demostraron que la inmovilización de  $\text{TiO}_2$  fue favorecida por la sinterización con el vidrio, bajo luz ultravioleta la razón de degradación de atrazina fue baja. La inmovilización de  $\text{TiO}_2$  sobre la superficie del vidrio aumentó al ser expuesta a tratamiento térmico y el estudio de difracción de rayos x confirmó la fase polimórfica anatase de las nano-partículas. En la deposición de  $\text{TiO}_2$  en la superficie del vidrio, la degradación de atrazina mostró una reducción bajo los límites de detección luego de 12h de exposición con una posible saturación del material después de 36 h de tratamiento. Finalmente, la razón de percolación disminuye al aumentar el tiempo de exposición y la temperatura. Por lo contrario la compresión incrementa a las mismas razones de sinterización.

Copyright © by

Amarillys Aviles Miranda

2016

**iv**

Amarillys Aviles-Miranda, 2016, thesis MS, UPR/RUM

“The important thing is to not stop questioning.

Curiosity has its own reason for existing”

-Albert Einstein

**v**

## ACKNOWLEDGEMENTS

It was a dream, it was a goal and today it is a reality!

Firstly, I want to thank God for giving me the strength, perseverance, and patience to pursue my master's degree. I am grateful to my advisors Pedro Tarafa and O. Marcelo Suarez for giving me the opportunity to be part of their research group and for the constant support. Thank the professor Felix Roman for allowing me to use his facility. To the USDA-NIFA and Trainings in Agriculture and Related Science (CETARS) program under grant N<sup>o</sup> 2011-38422-3083 and the National Science Foundation (NSF) under grants N<sup>o</sup>0833112 & 1345156 (CREST program) for supporting my research project.

In addition, I want to express gratitude to all my coworkers especially, Boris Renteria, Carlos Rivera, Perla Torres, and Victor Fernández for their advice and availability. Also, I want to recognize the undergraduate students, especially to Jonathan Ambrose, Claralys Hernández, Gerardo Nazario, Kelian Gonzáles, Liliana Hernández, Luis Larracuenta, Jorge De Jesús and Amanda Quintero for the hard work and collaboration which allowed them to be part of my success.

Finally, I want to thank my friends, my partner, and my family for the constant support, for the understanding and for the inspiration to achieve all my goals.

Thank you all!

Without all of you, this would not have happened

**vi**

## TABLE OF CONTENT

1	Introduction .....	1
1.1	Scope.....	2
1.2	Objectives .....	2
2	Literature Review .....	4
2.1	Water Pollution.....	7
2.2	Herbicides .....	7
2.2.1	Atrazine .....	10
2.3	Advanced Oxidation Process and TiO <sub>2</sub> .....	11
2.4	Photo-catalysis of TiO <sub>2</sub> and Atrazine Degradation .....	15
2.5	Recycled Glass .....	16
3	Methodology .....	18
3.1	Immobilization of TiO <sub>2</sub> nanoparticles by sintering on a glass substrate.....	18
3.2	Immobilization of TiO <sub>2</sub> Nanoparticles by Deposition and Heating onto Sintered Glass.....	19
3.3	Characterization of TiO <sub>2</sub> Nanoparticles by X-RAY Diffraction Analysis .....	21
3.4	Photo-degradation Studies of Atrazine.....	21
3.4.1	Useful Life of the TiO <sub>2</sub> / Glass Composite Material.....	23
3.5	Percolation Analyses.....	23

3.6	Compressive Strength Analysis .....	25
4	Results and Discussion.....	25
4.1	TiO <sub>2</sub> Immobilization .....	25
4.2	Characterization of TiO <sub>2</sub> by X-RAY Diffraction Analysis .....	29
4.3	Photo-degradation of Atrazine.....	31
4.3.1	Calibration Curve for the HPLC Unit.....	31
4.3.2	Treatability Studies with TiO <sub>2</sub> in Suspension, UV Light and Glass Substrate Effect.....	32
4.3.1	Treatability Studies for the TiO <sub>2</sub> / Glass Composite.....	34
4.3.2	Treatability Studies for Variable Atrazine Concentrations.....	36
4.3.3	Treatability Studies at Different Nanoparticles Size .....	38
4.4	Percolation Rate.....	41
4.5	Compressive Strength Analysis .....	44
5	Potential Application.....	45
6	Recomendations .....	45
7	Conclusions .....	46
8	References.....	47



## List of Tables

Table 1: Common herbicides, potential health effects and sources [31] .....	9
Table 2: Band gap in TiO <sub>2</sub> polymorphs.....	13
Table 3: Main by-products from atrazine degradation .....	16
Table 4: TiO <sub>2</sub> particle size and settling velocity in each suspension.....	27
Table 5: Size of the two different anatase nanoparticles .....	30
Table 6: Degradation rate constant for three different concentrations of atrazine .....	38
Table 7: Degradation rate constant for different TiO <sub>2</sub> particle sizes. ....	39
Table 8: Comparison of percolation rates for the glass filter and TiO <sub>2</sub> / glass composite material for the studied sintered parameters. ....	43

## List of Figures

Figure 1: Atrazine chemical structure .....	10
Figure 2: XRD spectra for the anatase and rutile polymorphic phases.....	14
Figure 3: (a) Glass sintered at 950°C for 45min, (b) glass sintered at 975°C for 75min.	17
Figure 4: Two layer composite immobilization method.....	21
Figure 5: Closed-box photo-reactor.....	22
Figure 6: Schematic of the percolation apparatus .....	24
Figure 7: Percentage (w/w) of TiO <sub>2</sub> nanoparticles immobilized on the sintered glass substrate by the deposition and heating method (water/ethanol suspension). .....	28
Figure 8: Percentage (w/w) of TiO <sub>2</sub> nanoparticles immobilized on the sintered glass substrate by the deposition and heating method (water/ acetic acid suspension). .....	28
Figure 9: XRD diffractogram for TiO <sub>2</sub> / glass composite heat treated at 900°C for 4 hours.....	30
Figure 10: Calibration curve for atrazine concentration in the HPLC unit.....	32
Figure 11: Atrazine levels after TiO <sub>2</sub> time exposure with and without UV light. ....	33
Figure 12: Atrazine levels under UV light and after had been in contact with the glass substrate (without TiO <sub>2</sub> ) in the absence of UV light.....	34
Figure 13: Atrazine levels with time after exposure to the TiO <sub>2</sub> / glass composite under UV light. ....	35

Figure 14: Atrazine degradation (%) per mass of TiO <sub>2</sub> immobilized on the two-layer TiO <sub>2</sub> / glass composite. ....	36
Figure 15: Atrazine levels for variable concentrations in contact with the TiO <sub>2</sub> / glass composite under UV light .....	37
Figure 16: Atrazine levels with the TiO <sub>2</sub> / glass composite embedded with a certain TiO <sub>2</sub> nanoparticle size. ....	39
Figure 17: Atrazine levels conducted in three different batches (12 hours each) for a single TiO <sub>2</sub> / glass composite exposed to UV light. ....	40
Figure 18: Performance map of percolation rate for the sintered glass substrates in (m <sup>3</sup> /s-m <sup>2</sup> ) as function of the sintering temperature and time. ....	41
Figure 19: Performance map of percolation rate for the sintered TiO <sub>2</sub> / glass composite in (m <sup>3</sup> /s-m <sup>2</sup> ) as a function of sintering temperature and time. ....	43
Figure 20: Performance map for the glass compressive strength as function of sintering temperature and time. ....	44

## List of Symbols and Abbreviations

TiO <sub>2</sub>	Titanium dioxide
AOPs	Advanced oxidation processes
•OH	Hydroxyl free radical
H <sub>2</sub> O <sub>2</sub>	Hydrogen peroxide
O <sub>3</sub>	Ozone
MCL	Maximum contaminant levels
CWA	Clean Water Act
EPA	Environmental Protection Agency
OHDEA	Hydroxydesethylatrazine
OH DIA	Hydroxydesisopropylatrazine
XRD	X-ray diffraction
SiO <sub>2</sub>	Silicon dioxide or silica
UTM	Universal testing machine
HPLC	High performance liquid chromatography
UV	Ultraviolet
CEC	Contaminants of emerging concern
ppb	Parts per billion
ppm	Parts per million
SEM	Scanning electron microscope
Na <sub>2</sub> O	Sodium dioxide or soda
CaO	Calcium oxide or lime

## List of Appendixes

Appendix A: Determination fo the settling velocity of the TiO <sub>2</sub> nanoparticles in suspension.....	52
Appendix B: Characterization of TiO <sub>2</sub> nanoparticles by XRD analysis .....	54
Appendix C: Pseudo reaction order of atrazine degradation .....	59

# 1 Introduction

Water pollution is becoming one of the most challenging problems faced by Humankind worldwide. In particular, herbicides from agricultural activities have become serious pollutants that can reach and disturb water supply sources. Herbicides can be natural or man-made organic compounds used to control weeds and pests; they can have low degradation rates in natural environments, remaining in their surroundings for long periods of time [1]. Moreover, as water moves through runoffs and percolation, it transports these contaminants via surface water bodies into urban areas or groundwater reservoirs, which affected the US drinking water sources quality [2]. This is why a direct relationship between herbicide use and the presence of toxic compounds (contaminants) in surface water and groundwater has been found.

One of the most widely used and well-known herbicides is atrazine, which can be degraded by an advanced oxidation processes (AOPs) in surface waters [3]. Recent studies have evaluated the potential of semiconductors to promote oxidation of organic contaminants [1]. One of those appealing alternative photocatalytic compounds is titanium dioxide ( $\text{TiO}_2$ ). It is one of the most efficient photo-activated semiconductors with no negative effect on humans or the environment, and bears high thermal and chemical stability [3]. Hence, the present study focused on assessing the viability of a  $\text{TiO}_2$ -containing substrate to effectively photo-degrade atrazine in water solutions. The methodology encompasses the immobilization of  $\text{TiO}_2$  particles, rather than the use of  $\text{TiO}_2$  suspensions, in sintered glass as the solid matrix. Crushed, recycled glass is

proposed as an alternative material in order to reduce waste generation and environmental impacts.

## **1.1 Scope**

The scope of this research is to develop and establish an immobilization technique to fix TiO<sub>2</sub> nanoparticles onto a porous, solid substrate made of crushed, recycled glass for the degradation of atrazine. The ultimate goal is to set the foundations for the development of a porous photo-activated media for water pollutant filtering.

## **1.2 Objectives**

To achieve the scope the following objectives were established in this research:

- Immobilized TiO<sub>2</sub> nanoparticles in a solid, porous matrix using recycled, crushed glass as the main substrate evaluating two physical techniques.
  - Sintering together both the TiO<sub>2</sub> and the crushed glass particles
  - Deposition of the TiO<sub>2</sub> nanoparticles from a suspension onto a whole sintered glass surface and subsequent heat treatment.

- Evaluate the TiO<sub>2</sub> / glass composite capacity for the degradation of atrazine under the influence of ultraviolet (UV) light by means of high performance liquid chromatography (HPLC) analyses.
- Analyses of water percolation and compressive strength as an important thermo-mechanical property.



## 2 Literature Review

Water, an essential resource for life, represents 75% of the earth surface and is known as the universal solvent. However, less than 3% of all the water in world is classified as freshwater, which makes it a limited resource for human consumption and domestic uses. Moreover, these limited freshwater resources are being threatened by the intrusion of undesired water pollutants, including contaminants of emerging concern (CEC). Some of these pollutants are herbicides that once trapped in the soil, are driven away by surface runoffs or groundwater flow, which eventually end up in water bodies such as rivers, lakes and aquifers. One of these herbicides is atrazine. Accordingly, this section provides a literature review regarding the occurrence, distribution, environmental impacts, health effects, and current and proposed technologies for treatment/destruction of atrazine in water.

Atrazine, a chemical compound created to improve land liberation in agriculture activities, is one of the most used herbicides around the world [4]. In the US, 20 superfund sites have been detected with atrazine concentrations up to 61.6 part per billions (ppb) [5]. Liu et al. [6] also reported 38.6 ppb of atrazine in rivers in Missouri and Nebraska, 224 ppb in Atlanta, and 300 ppb in Iowa. These contaminant can affect a drinking water exceeding the maximum contaminant levels (MCL) established by the US Environmental Protection Agency (EPA) of 3 ppb. Furthermore, since it is associated with human reproductive disorders and birth effects [7], some European countries banned the use of atrazine while in the US and other countries its use continues [8].

The natural degradation of atrazine in water by enzymatic action takes place in within days for aerobic conditions or in years by anaerobic paths[4], [9]. In this adverse context, the advanced oxidation process of atrazine is an alternative to accelerate the degradation process. This process consists on the oxidation of persistence organic matter by free radicals that can be generated by the combination of ozone, hydrogen peroxide, UV light, semiconductor, or other sources [10]. Recently, semiconductive materials combined with UV light sources have emerged as an attractive alternative to degrade organic matter. One of these semiconductors is  $\text{TiO}_2$ , which acts as a photocatalytic agent with UV light excitation the oxide induces the formation of hydroxyl ( $\cdot\text{OH}$ ), a free radical that compares with hydrogen peroxide ( $\text{H}_2\text{O}_2$ ) and ozone ( $\text{O}_3$ ) as the most potent and useful reactive radicals [11], to effectively oxidize/degrade organic compounds in water. From all three naturally occurring  $\text{TiO}_2$  polymorphs, the anatase phase is the one that was found to bear the higher photo-activity capacity, as it generates the higher recombination of excited electrons in the catalysis of organic compounds [12].

Numerous researches have been studied the degradation capacity of atrazine using  $\text{TiO}_2$  nanoparticles. Some findings demonstrated 20 min of half-life of atrazine using suspended  $\text{TiO}_2$  nanoparticles in water under UV light [13], [14]. This efficiency is attributed by the large  $\text{TiO}_2$  active sites. However, this approach creates another problem in the water purification process due to the residual  $\text{TiO}_2$  colloidal particles yielding high turbidity [15]. Hence, this drawback has caused an increasing interest in the development of new approaches including immobilization of  $\text{TiO}_2$  nanoparticles on

solid matrices for the destruction of organic compounds in water. This alternative promotes easy recovery and re-use of the nanoparticles.

Different methods can render the immobilization of the nanoparticles. One of them consists of the deposition and immobilization of the nanoparticle on a solid substrate. Typically this is performed by the dispersion of the nanoparticles during the synthesis of a polymer [16]. Singh et al. [17] report a degradation rate of methylene blue dye up to 90% in 6 hours of UV light exposition. However, some disadvantages are limitations in light penetration, long exposure needed under UV light, and the conditions of the surface [3], [18].

Other method consists of the oxide deposition onto a solid substrate and its subsequent immobilization by the heat treatment. Some techniques used are self-assembling [19], sol-gel dip coating [18], [20], solution casting [15], and sputtering [21]. In all of these cases the oxide nanoparticles are immobilized by heat treatment. Some degradation analysis using the nanoparticles immobilization on a substrate demonstrated 94% of atrazine degradation for 70 to 90 min using synthesized TiO<sub>2</sub> nanoparticles supported over the surface of boron waste particles [22] or on phosphorus particles [23].

In this research the TiO<sub>2</sub> nanoparticles were immobilized with a recycled glass substrate to degrade atrazine in water. The deposition and the immobilization of the nanoparticles were performed by sintering together both the TiO<sub>2</sub> and the crushed glass particles and by deposition of the TiO<sub>2</sub> nanoparticles from a suspension onto a whole sintered glass surface and subsequent heat treatment.

## **2.1 Water Pollution**

The main pollution of water sources is caused primarily by anthropogenic effects. They are classified in two broad categories: point and non-point sources. Point source pollution refers to water pollution that comes from a single point and is usually regulated, while non-point source denotes pollution that comes from non-regulated discharges delivered indirectly through transport or environmental change such as land runoff or precipitation. The main pollutants from point sources are by-products of industrial and laboratory discharges, sewage water, medical waste, and domestic waste [24], which are contained and enforced by the Clean Water Act (CWA) of 1972 [25]. The current list of priority pollutants divulged by CWA includes 126 pollutants such as benzene, chloroethane, chloroform, ethylbenzene, naphthalene, nitrobenzene, phenol, pyrene, toluene, arsenic, copper, 4,4-DDT, among others [26]. In contrast, non-point sources are deliberate and non-controlled discharges as the excessive use of herbicide in agriculture activities.

## **2.2 Herbicides**

Herbicides are pesticides, organic matter-based, used to control undesired weeds or plants [27]. They are made up of chemical compounds that can be natural or man-made. The use of herbicides improves the agriculture economy by the increment in efficient labor work. In the 1940s one of the first herbicides created was 2, 4-D (2,4-

dichlorophenoxyacetic acid) [28]. After this invention, science continued to develop this industry and today more than 400 herbicides are used over the world. Some advantages of the herbicides application are the increment of food supply and the faster liberation of the land [27]. In contrast, some disadvantages are soil and water pollution that can impact water supply sources quality.

The EPA under the Safe Drinking Water Act (SDWA) has established MCLs for different herbicides. A list of the most common herbicides with their MCLs and potential health effects is presented and summarized in Table 1.

Table 1: Common herbicides, potential health effects and sources [29]

<b>Contaminant</b>	<b>MCL (mg/L)</b>	<b>Potential Health Effects</b>	<b>Sources of Contaminant in Drinking Water</b>
Alachlor	0.002	Eye, liver, kidney; anemia; risk of cancer	Runoff from herbicide
Atrazine	0.003	Cardiovascular system or reproductive problems	Runoff from herbicide
2,4-D	0.070	Kidney, liver, or adrenal gland problems	Runoff from herbicide
Dalapon	0.200	Minor kidney changes	Runoff from herbicide
Dinoseb	0.007	Reproductive difficulties	Runoff from herbicide
Diquat	0.020	Cataracts	Runoff from herbicide
Endothall	0.100	Stomach and intestinal problems	Runoff from herbicide
Ethylbenzene	0.700	Liver or kidneys problems	Discharge from petroleum refineries
Glyphosate	0.700	Kidney problems; reproductive difficulties	Runoff from herbicide
Picloram	0.500	Liver problems	Herbicide runoff
Simazine	0.004	Problems with blood	Herbicide runoff
2,4,5-TP (Silvex)	0.050	Liver problems	Residue of banned herbicide

### 2.2.1 Atrazine

For the sake of brevity, we limited our study to one representative herbicide; atrazine (6-chloro-N-ethyl-N-(1-methylethyl)-triazine-2,4-diamine), because it is widely used in the US and is a persistent pollutant in the environment. Atrazine is a member of the chloro-*triazine* herbicide family (refer to Figure 1 for its chemical structure) registered in 1952 by DuPont Manufacturing. It is estimated that the atrazine application ranges from 70,000 to 90,000 tons per year in the world [30].

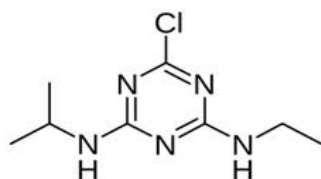


Figure 1: Atrazine chemical structure

Atrazine is mainly used to control pest in grain crops such as corn and rice [31]. Upon application, it accumulates in the leaves of the weeds acting as inhibitor of the photosynthesis process [32]. In this process, the singlet chlorophyll energy is dissipated to the center of the protein of the plant membrane and the accumulation of the chlorophyll initiated the lipid per-oxidation process (free radicals) that eventually destroys the plant [9], [33]. Atrazine has relatively high solubility in water [30] and, hence, the excess of atrazine not absorbed by the plant and left in the soil, may cause contamination of surface water by run-off action. These sources of water feed the treatment plant and can affect the drinking water quality. In humans, the exposure of

atrazine is associated with defects in reproductive system and birth effects such as low fetal weight, and heart and urinary problems. It can gain access to the human body through inhalation, oral and/or dermal paths. However, inconsistent information is found related to cancer [32].

The natural degradation of atrazine by enzyme or bacteria action demonstrates better degradation in aerobic than anaerobic conditions with half-life of 60 to 150 days and 660 days, respectively, for loamy soil [4]. Hequet et al. [13] reported that atrazine may undergo photo-degradation at UV light wavelengths ranging from 220 to 260 nm. In this research hydroxyatrazine (OHA) was found as the main metabolite for the said wavelengths. A possible homolytic cleavage of C-Cl bond occurred during the degradation. Some others metabolites in the natural degradation by UV light exposure are: hydroxydesethylatrazine (OHDEA) and hydroxydesisopropylatrazine (OHDIA).

In summary, the slow degradation rate of atrazine in natural environments is also associated with the lack of natural sources with wavelengths from 220 to 260 nm and the limitations of conventional water treatment plants. In this context, the advanced oxidation process (AOP) emerges as an alternative for the degradation/destruction of atrazine in water [34].

### **2.3 Advanced Oxidation Process and TiO<sub>2</sub>**

The AOP is an alternative for the degradation of persistent pollutants, which are difficult to remove with conventional water treatment processes [11]. This process is



largely studied for different applications and represents an important alternative for water, air, and soil treatment to eliminate or reduce the pollutant impact in the environment [35]. The main goal has been to achieve the complete mineralization of the contaminant and their intermediates. In this process, the UV or visible light source is present along with an oxidant species and a catalytic material to create a free radical, hydroxyl groups ( $\cdot\text{OH}$ ), as a chemical initiation to decompose organic pollutants [36]. Some oxidant species can be  $\text{O}_3$  and  $\text{H}_2\text{O}_2$ , which, under UV light irradiation, produce free radicals that are inefficient for the total degradation of organic compounds [37]. An alternative to improve degradation is the combination of a nanosized semiconductor (as  $\text{TiO}_2$ ) with UV light to generate ( $\cdot\text{OH}$ ) and, thus, promote the total target contaminant oxidation.

$\text{TiO}_2$  is a semiconductor material with high photo-catalytic capacity driven by light and able to photo-degrade persistent organic pollutants in water [3]. It has been used in multiple applications and industries such as food, paints, toothpaste, cosmetic, and water and air treatment, among others [12].  $\text{TiO}_2$  is one of the most efficient photo-activated semiconductors with no negative effect for humans or the environment, and bears high thermal and chemical stability [38], [39]. Intensive research seeks to improve its capacity and to incorporate it in water treatment processes.

$\text{TiO}_2$  exists in three polymorphic structures: two metastable structures known as anatase and brookite, and one stable structure at atmospheric pressure known as rutile [21]. The photo-activity capacity of the  $\text{TiO}_2$  is promoted by the polymorph type. Anatase has the higher activation capacity represented by the higher experimental band gap

compared to rutile (Table 2). This property increases the probability of higher density of open space, better catalysis process, and higher degradation rate of pollutants. Moreover, brookite has barely been studied due to its complex synthesis. The TiO<sub>2</sub> structure is a function of temperature and time with irreversible transformation. The reported transition temperature of anatase to rutile varies between 400°C to 1,200°C [12].

Table 2: Band gap in TiO<sub>2</sub> polymorphs

Phase	Anatase	Rutile
Band gap energy (eV)	3.2	3.0

The structure transformation and the size of the nanoparticles can be assessed by XRD. Figure 2 displays the XRD spectra expected for anatase and rutile with their corresponding main diffraction peaks (crystallographic planes). To obtain the spectra the TiO<sub>2</sub> nanoparticles were deposited onto recycled glass and evaluated without heat treatment (anatase) and after 1000°C for 3 hours of heat exposition (rutile).

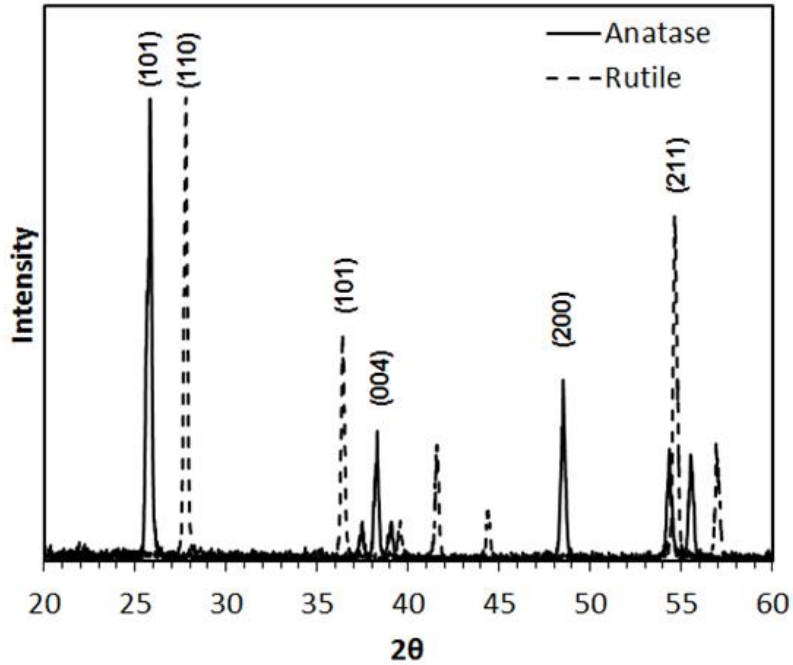


Figure 2: XRD spectra for the anatase and rutile polymorphic phases

Further, the size of the crystals can be approximated with Scherrer's formula (Eq.1), which relates the crystallinity with the size of nanoparticles.

$$\tau = \frac{0.9\lambda}{\beta \cos\theta} \quad [1]$$

Where,  $\tau$  is the mean crystallite size (nm),  $\lambda$  is x-ray wavelength (nm),  $\beta$  is the width at half the maximum intensity, denoted FWHM (radians), and  $\theta$  is the Bragg angles (radians).

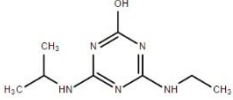
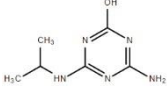
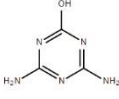
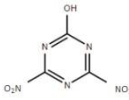
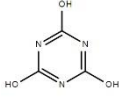
## 2.4 Photo-catalysis of TiO<sub>2</sub> and Atrazine Degradation

During the photo-activation of TiO<sub>2</sub> with a UV light, the electrons are excited from a valence band to a conductive band creating an open space in the valence band which promotes the adsorption and oxidation of water and oxygen molecules. This process occurs on the catalytic surface of the particles, promoting the formation of hydroxyl free radicals that decompose organic pollutants [1]. An example of these redox reactions in the presence of water are shown in the following reactions (Eqs. 2 - 5) where the excited electron is represent as (e<sup>-</sup>) and the open space in the valence band as (h<sup>+</sup>) [12].



Of particular interest for this study is atrazine, which can be degraded by these free radicals that help degrade the target compound into simpler molecules. This degradation in the presence of UV light consists of dealkylation, deamination, and dechlorination processes until reaching its last by-product, cyanuric acid which continues to be an undesirable contaminant in water [30]. Table 3 shows the main by-products generated by atrazine degradation [39].

Table 3: Main by-products from atrazine degradation

Name of compounds	Structure
2-Hydroxy-4-ethylamino-6-isopropylamino-s-triazine	
2-Hydroxy-4-amino-6-isopropylamino-s-triazine	
2-Hydroxy-4,6-diamino-s-triazine	
2-Hydroxy-4,6-dinitro-s-triazine	
2,4,6-Trihydroxy-s-triazine	

## 2.5 Recycled Glass

This research aims at developing a new methodology to lower atrazine levels in water while sustaining and regenerating our natural resources. One way to achieve this is by creating alternative applications of recyclable products. Hence, we proposed the construction of a low cost TiO<sub>2</sub>-based composite made of sintered recycled glass doped with TiO<sub>2</sub> for the degradation of atrazine. Glass was selected because it is one hundred percent recyclable with no loss of purity or quality [40]. In addition, it is inert, relatively inexpensive, and durable based on SiO<sub>2</sub>-Na<sub>2</sub>O-CaO [41]. The type of crushed glass

employed for the research was MG-30. This kind of glass is a functional fine aggregate material made out primarily from curbside pick-up. The particles are between 0.30 to 0.70 mm (30-70 Mesh). The crushed glass is compacted by sintering process to create a solid, porous material with a circular shape.

Sintering process is a technique by which a solid mass of material is formed by heat or pressure treatment process from many smaller pieces [42]. The particles will join together and the free spaces, porosity, will reduce as shown in Figure 3. To obtain the imagen a scanning electron microscope (SEM) JSM-6390 was used and processed in an Image J program. The typical temperatures used in heat treatment, which is used in the current study, are approximately 50% to 80% of a material's melting temperature.

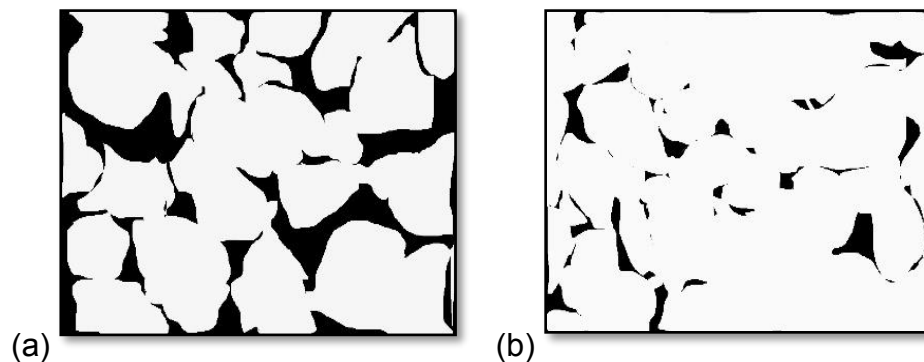


Figure 3: (a) Glass sintered at 950°C for 45min, (b) glass sintered at 975°C for 75min.

The sintering process is divided in different categories depending of the system. Viscous sintering defines the sintering process for amorphous material, such as glass, where the matter transport occurs by viscous flow. Deformation of the particles occurs by neck growth and densification while the strength of the particles compact increases. Rahaman defined the model to explain the grain growth, neck growth and cluster

between particles which occurs in amorphous material [42]. The process was found to occur by the surface diffusion and migration of the particles boundaries. Differences in the initial size of the particles accelerated the boundary migration rate as the boundary swept through smaller grain.

After sintering, important mechanical properties are affected as percolation capacity and compressive strength. In this research these two properties were studied at different sintering conditions (i.e. temperature and time) to determine the viability and further implementation of this technology for water filtering which also, be able to support the TiO<sub>2</sub> nanoparticles for the degradation polluted organic matter as atrazine under the influence of the UV light.

### **3 Methodology**

#### **3.1 Immobilization of TiO<sub>2</sub> nanoparticles by sintering on a glass substrate**

Crushed recycled glass particles, MG-30 type, were used to produce a solid substrate by a sintering process. This process sought to create a porous, compact glass material able to support/immobilize TiO<sub>2</sub> nanoparticles while allowing water percolation. The following paragraphs present the methodology used to prepare the materials studied in this thesis.

First, we placed thirty grams (30 g) of MG-30 and 0.33 g of  $\text{TiO}_2$  in a beaker with 25 mL of ethanol (33% v/v) and 50 mL of water. The suspension (particles + solvents) was then stirred vigorously and placed on a hot plate at  $60^\circ\text{C}$  to evaporate the solvent. Finally, the blended particles were transferred into a circular ceramic mold (0.05m internal diameter) and placed inside a high temperature muffle furnace for the sintering process. The ceramic mold was lined with a layer of ceramic wool to prevent glass adhesion onto the mold upon heating. Three sintering temperatures ( $750^\circ\text{C}$ ,  $775^\circ\text{C}$  and  $800^\circ\text{C}$ ) and three sintering times (20, 25, and 30 min.) were used. After sintering, the mold was removed from the muffle furnace and allowed to cool at room temperature. After cooling, the sintered composite mixture (i.e.  $\text{TiO}_2$  / glass composite) was removed from the ceramic mold. The final  $\text{TiO}_2$  / glass composite was approximately 0.013m thick and 0.05m in diameter.

### **3.2 Immobilization of $\text{TiO}_2$ Nanoparticles by Deposition and Heating onto Sintered Glass**

After preparing the glass substrates these were covered with  $\text{TiO}_2$  nanoparticles. The whole glass substrates were obtained by sintering 30 g of MG-30 crushed glass. The sintering procedure was the same as the one described above except that no  $\text{TiO}_2$  particles were added upon glass sintering. The sintering temperature employed for this process was  $963^\circ\text{C}$  for 60 min. After cooling, the glass substrate was cleaned by



dipping it into a solution of phytic acid (3g/L) for one hour and then dried in an oven at 60°C.

The deposition of the TiO<sub>2</sub> particles onto the glass substrate surface was carried out by sedimentation. The TiO<sub>2</sub> suspension was prepared by adding 4.0 g of TiO<sub>2</sub> to a water solution containing either acetic acid or ethanol (33% v/v). A hot plate magnetic stirrer helped homogenize the suspension for 15 min. Then the suspension was transferred to a jar having four glass substrates at the bottom. The jar was left resting on a hot plate inside a hood for 24h. During this period the TiO<sub>2</sub> particles were expected to settle on the glass substrate surface. After the 24 h settling period, the jar was heat to 60°C for 18 hours to evaporate the solvent and the two layer composite material was developed as show Figure 4. As stated earlier, two different solvents (acetic acid and ethanol) were evaluated to analyze the impact on the settling process. Our purpose was to understand the deposited particles distribution for each solvent. Hence, the size of the TiO<sub>2</sub> particles in the suspension with each solvent was measured by a Zeta Sizer Nano-ZS90 instrument.

In order to effectively fix/attach the TiO<sub>2</sub> particles already deposited, the glass substrates were then placed in a muffle-furnace at different temperatures and times for each solvent, i.e. 600°C and 900°C for 2 and 4 hours. Control condition was a reference sample with deposited nanoparticles onto the glass surface but not heat treatment. After heating, the sintered composite (i.e. TiO<sub>2</sub> / glass composite) were let cool at room temperature and washed with water in agitation tree times. The substrates

are then dried in an oven at 60°C for 24h. The mass of TiO<sub>2</sub> finally attached/immobilized onto the glass substrate was measured by difference in weight.

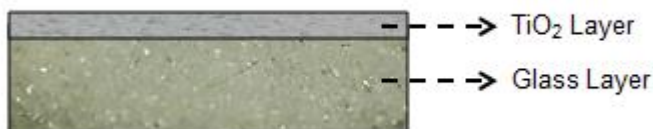


Figure 4: Two layer composite immobilization method

### 3.3 Characterization of TiO<sub>2</sub> Nanoparticles by X-RAY Diffraction Analysis

According to the literature and as mentioned before, the polymorph structure and, the photo-activation capacity of the TiO<sub>2</sub> nanoparticles change as they are exposed to high temperatures. The objective of the ensuing XRD analysis was then to characterize the TiO<sub>2</sub> phase of the nanoparticles after the sintering process and to estimate the particle size via the Scherrer equation (Eq. 1). The sintered samples (at different temperatures and times) were evaluated using D 5000 x-ray diffraction unit over a  $2\theta$  range of 15-75° with 0.02° steps and 2.5 s of dwelling time.

### 3.4 Photo-degradation Studies of Atrazine

The photo-degradation study was designed to evaluate the viability of the sintered composite materials doped with TiO<sub>2</sub> nanoparticles to degrade atrazine under UV light. We first prepared the atrazine concentrations (0.025 ppm to 0.25 ppm) from a

lab-grade solution (Supelco, Bellefonte PA) of 1000 $\mu$ g/mL. These atrazine solutions were then analyzed in a HPLC instrument (Agilent Technologies series 2000 unit) in order to observe the instrument response and to construct a calibration curve. The analysis was performed in a BDS Hypersil C-18 (100 x 4.6 mm) column operated at 30.0 $^{\circ}$ C with a mobile phase of 1.0mL/min at 65% of methanol and 35% of water. The injection volume was 50 $\mu$ L and a UV light detector was operated at 222nm.

For the treatability study a closed-box photo-reactor (to avoid external light intrusion) designed to house a beaker/recipient and a UV light source (refer to Figure 5) was used. The atrazine solution was placed in contact with the sintered composite material (having the immobilized TiO<sub>2</sub>) inside the photo-reactor box and then we turned on the UV light ( $\lambda = 365$  nm and intensity, 1000 W/cm<sup>2</sup>). The atrazine solution was permanently stirred while the treatability study is in progress (periods ranging from 2 to 12 hours). The atrazine solution was sampled every 30 min to 2 hours; The residual atrazine levels were then measured in the HPLC.

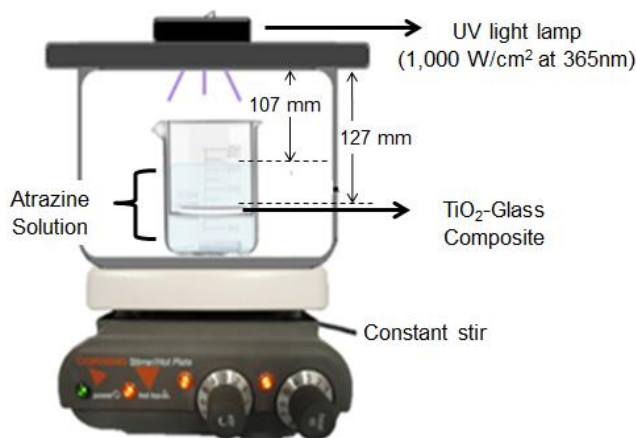


Figure 5: Closed-box photo-reactor.

### 3.4.1 Useful Life of the TiO<sub>2</sub> / Glass Composite Material

The capacity for the TiO<sub>2</sub> / glass composite to degrade atrazine for long time periods bearing similar degradation yields describes its useful life. Hence, this experimental set was designed to assess the useful life of a single TiO<sub>2</sub> / glass composite by placing it in contact with a new atrazine solution of 0.10 ppm every 12 h while repeating the treatability study. The degradation yield was quantified and its effectiveness upon exhaustion. A triplicate analysis was performed.

## 3.5 Percolation Analyses

Percolation is defined as the ratio of change in water volume with time through a porous media. Since the ultimate goal of this endeavor is the development of a filter media able to degrade organic contaminants, the evaluation of the percolation capacity of the porous glass sintered is mandatory. Hence, we examined the percolation rate as a function of both sintering temperature and time for all glass composites. To this purpose we recorded the elapsed time it took for a given volume of water to flow through the composite filter employing a custom-made percolation apparatus shown in Figure 6. This apparatus had a PVC pipe with an adapter to store the sample. A funnel (at the top of the pipe) helped keep a constant hydraulic head. The whole system along with the composite sample was sealed with silicone to avoid water leaks. Before conducting the percolation test, the composite is first immersed in water for one hour to

saturate it. Finally, the water was fed into the system and the time for the water volume to percolate was recorded. An average of three experiments for each sample was reported.

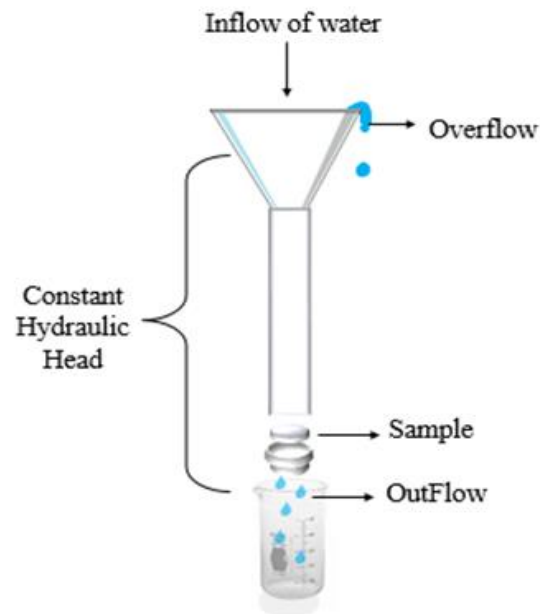


Figure 6: Schematic of the percolation apparatus

The percolation rate was then calculated by the relationship presented in Eq. 6 where the area is the composite area normal to the water flow.

$$\text{Percolation rate} = \text{Volume (gal)} / [\text{Time (min)} * \text{Area (ft}^2\text{)}] \quad [6]$$

### 3.6 Compressive Strength Analysis

The compressive strength value indicates the material's capacity to withstand gradual compression loads before fracture. This analysis was performed for the set of glass substrates sintered at 950°C, 963°C and 975°C for 45, 60, and 75 min. The compression specimens had a cross section of 1 cm x 1 cm and were obtained from the center of each sintered glass substrate. They were tested in an Instron universal testing machine (UTM) with a loading cell capacity of 25 kN.

## 4 Results and Discussion

### 4.1 TiO<sub>2</sub> Immobilization

TiO<sub>2</sub> nanoparticles were fixed or immobilized on the sintered glass substrate by two methods. The first one immobilized the nanoparticles by sintering together both the TiO<sub>2</sub> nanoparticles and the crushed glass particles in order to formulate a **combined TiO<sub>2</sub> / glass composite**. In the second method the TiO<sub>2</sub> nanoparticles are immobilized by deposition and subsequent heat treatment. The said deposition consisted of gravitational deposition of TiO<sub>2</sub> nanoparticles from a suspension onto a whole sintered glass surface, ending with a **two-layer TiO<sub>2</sub> / glass composite**.

The amount of TiO<sub>2</sub> been immobilized in the combined TiO<sub>2</sub> / glass composite was determined assuming that the entire mass employed had been trapped within the

glass substrate during the sintering process. However, in the two-layer TiO<sub>2</sub> / glass composite, the amount of TiO<sub>2</sub> immobilized was determined by another method: the difference in weight of the sintered glass substrate before and after the deposition and heating procedure. As stated in the Methodology section, the TiO<sub>2</sub> deposition was achieved by submerging a whole sintered glass substrate into a TiO<sub>2</sub> suspension left at rest. We evaluated two different suspensions: (1) water/ethanol/TiO<sub>2</sub>; and (2) water/acetic acid/TiO<sub>2</sub>.

Figures 7 and 8 shows the final TiO<sub>2</sub> mass (in percentage) been immobilized in the sintered glass surface employing the TiO<sub>2</sub> suspensions with ethanol and acetic acid, respectively. Table 4 presents the measured TiO<sub>2</sub> particle size and the settling velocity attained in each suspension. According to our results, the final mass of TiO<sub>2</sub> immobilized on the glass substrate increased with heating temperature and time. This could be attributed to the partial viscous flow of the glass surface during the heat treatment, which can attach/bond the TiO<sub>2</sub> nanoparticles to the glass during the solidification process. Also, the higher mass of TiO<sub>2</sub> was immobilized when ethanol was present in the suspension rather than acetic acid.

It is believed that the acetic acid increased the suspension ionic strength, hence, promoting TiO<sub>2</sub> particles agglomeration and a particle size increase, as seen in Table 4. The larger the particle size, the higher the settling velocity as stated by Stokes' law for a discrete particle. Thus, a particle exhibiting a large settling velocity will promote a less uniform deposition over the glass substrate. Conversely, smaller particle sizes (as seen when using ethanol) will settle more slowly leading to a more uniform TiO<sub>2</sub> layer over

the glass substrate. This concept may be supported by computing the settling velocity of the particles (Appendix A), which is described in Equation 7 and presented in Table 4.

$$V_s = (g/18\mu)(\rho_s - \rho)d_p^2 \quad [7]$$

where,  $g$  is the gravitational constant ( $9.8 \text{ m/s}^2$ );  $\mu$  is the viscosity of the suspension ( $\text{kg/m-s}$ );  $\rho_s$  is the density of the particle ( $\text{kg/m}^3$ );  $\rho$  is the density of the suspension ( $\text{kg/m}^3$ ); and  $d_p$  is the diameter of the particle (m). In addition to the settling velocity, one can expect that smaller  $\text{TiO}_2$  particles can accommodate easier into the glass substrate pores than large settled particles. Naturally, the smaller the particle size, the larger the surface area. Hence, this will increase the interactions between the glass and  $\text{TiO}_2$ , which tend to be higher for small particles than for large particle sizes [43].

Table 4:  $\text{TiO}_2$  particle size and settling velocity in each suspension

<b>Suspension</b>	<b><math>\text{TiO}_2</math> Particle Size (nm)</b>	<b>Settling Velocity (<math>\mu\text{m/s}</math>)</b>
Water/Ethanol/ $\text{TiO}_2$	365	0.144
Water/Acetic Acid/ $\text{TiO}_2$	729	0.743

Since the  $\text{TiO}_2$  immobilization technique, i.e. gravitational deposition with ethanol heated at  $900 \text{ }^\circ\text{C}$  for 2 h, acquired the highest immobilization capacity, the photo-degradation of atrazine and percolation rate studies were performed on these samples.



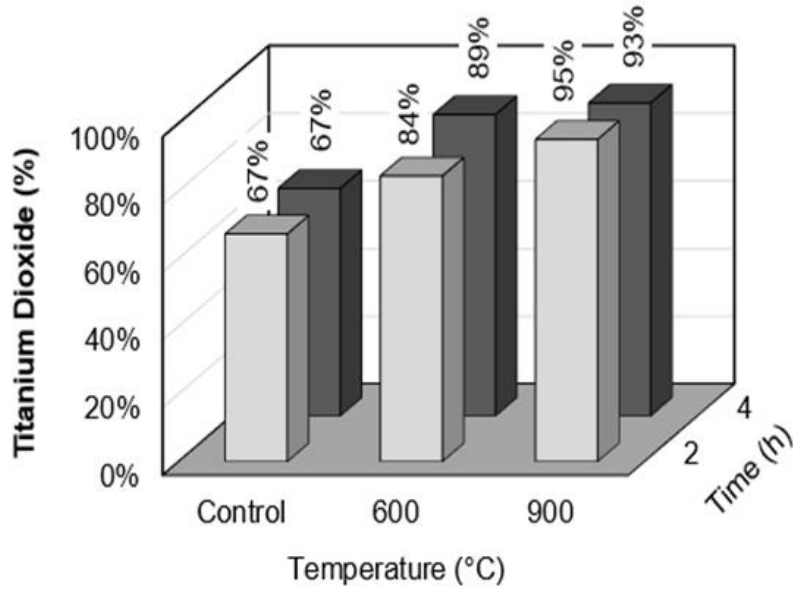


Figure 7: Percentage (w/w) of TiO<sub>2</sub> nanoparticles immobilized on the sintered glass substrate by the deposition and heating method (water/ethanol suspension).

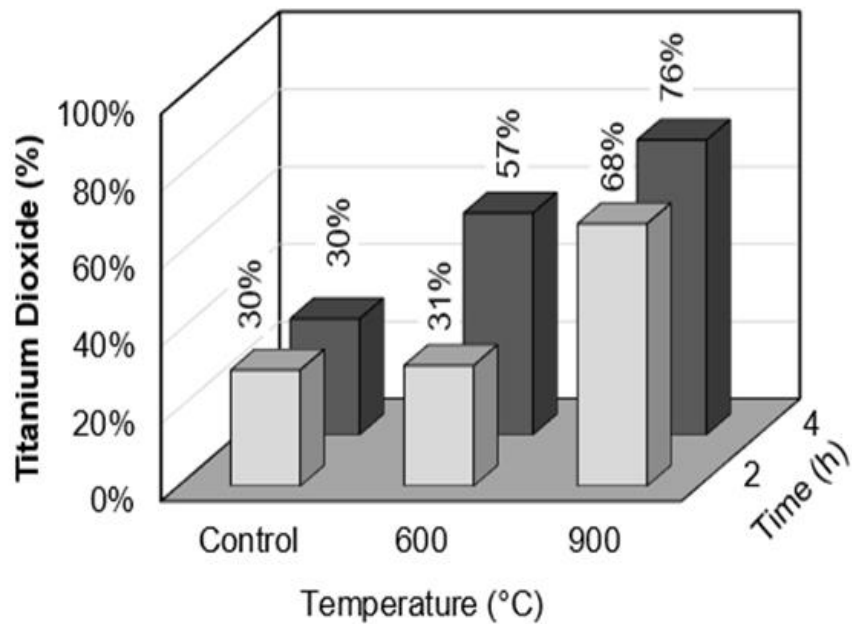


Figure 8: Percentage (w/w) of TiO<sub>2</sub> nanoparticles immobilized on the sintered glass substrate by the deposition and heating method (water/ acetic acid suspension).

## 4.2 Characterization of TiO<sub>2</sub> by X-RAY Diffraction Analysis

An XRD analysis allowed characterizing the TiO<sub>2</sub> structure after thermal exposure. Figure 9 presents the XRD diffractogram obtained from a two-layer TiO<sub>2</sub> / glass composite after undergoing a thermal treatment at the highest temperature and longest time we used in the immobilization process (900°C for 4 h). The results show a peak near  $2\theta = 25.60^\circ$ , which according to the literature is characteristic of (101) plane of the anatase polymorph [12]. This finding led us to conclude that no TiO<sub>2</sub> phase change occurred upon the thermal treatment employed for the deposition and heat immobilization method. Anatase is the desired phase, since it presents the higher TiO<sub>2</sub> photo-activation capacity by the high adsorption of the oxygen molecule and efficient formation of electron-hole pairs during the catalysis process [44]. Appendix B part a and b provides additional XRD diffractograms conducted for the TiO<sub>2</sub> exposed at other conditions of temperature and time.

The crystallite size (nm) of the nanoparticles was estimated using the Scherrer's formula (Eq.1) from the XRD diffractogram. Table 5 presents the data for each crystallographic plane in the anatase structure where the intensive peak suggests an approximate crystallite size of 32 nm.

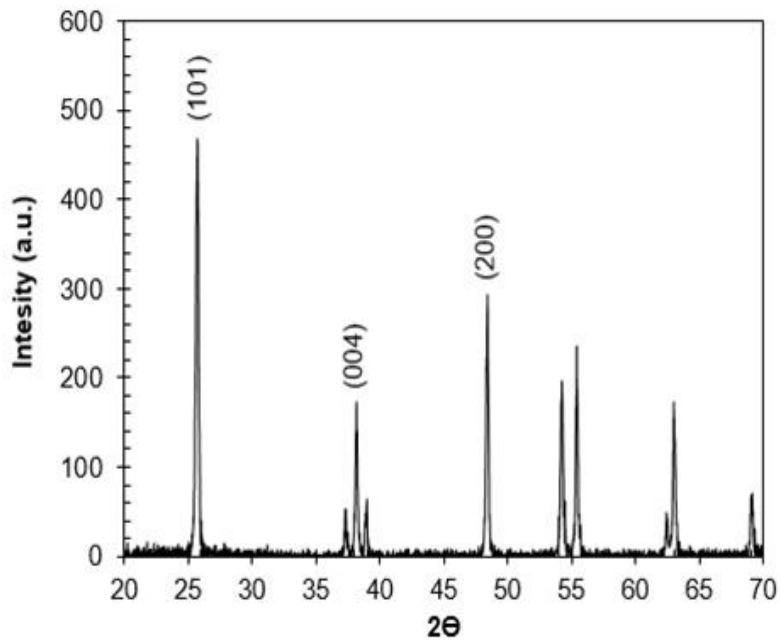


Figure 9: XRD diffractogram for TiO<sub>2</sub> / glass composite heat treated at 900°C for 4 hours.

Table 5: Size of the two different anatase nanoparticles

<b>2θ</b>	<b>λ (nm)</b>	<b>β (radians)</b>	<b>Crystallite size (nm)</b>
25.79	0.35	0.31	<b>32</b>
38.25	0.24	0.27	40
39.05	0.23	0.27	39
48.50	0.19	0.28	38
54.36	0.17	0.30	36
55.52	0.17	0.30	36
63.16	0.15	0.39	27

### 4.3 Photo-degradation of Atrazine

Atrazine, a persistent herbicide, was used as the model herbicide to challenge the TiO<sub>2</sub> / glass composite degradation potential. An HPLC unit allowed detecting and reading atrazine concentrations after treatment.

#### 4.3.1 Calibration Curve for the HPLC Unit

Diluted atrazine solutions ranging from 0.050 to 0.250 ppm were prepared to create a calibration curve for the HPLC unit. Figure 10 shows a direct relationship between the standard atrazine concentration and the area detected by the HPLC depicted in the chromatogram. A linear regression model obtained is presented in Equation 8 with a correlation coefficient of  $R^2 = 0.9999$ . This expression was used to determine unknown concentration of atrazine as a function of the HPLC response.

$$y = 606.53 x - 1.1838 \quad [8]$$

where,  $x$  is the concentration of atrazine in solution (ppm) and  $y$  represent the area under the curve depicted in the chromatogram (AU \*s). The area is obtained from the product of the instrument intensity (AU), which was obtained by the height of the peak, and the retention time (s).

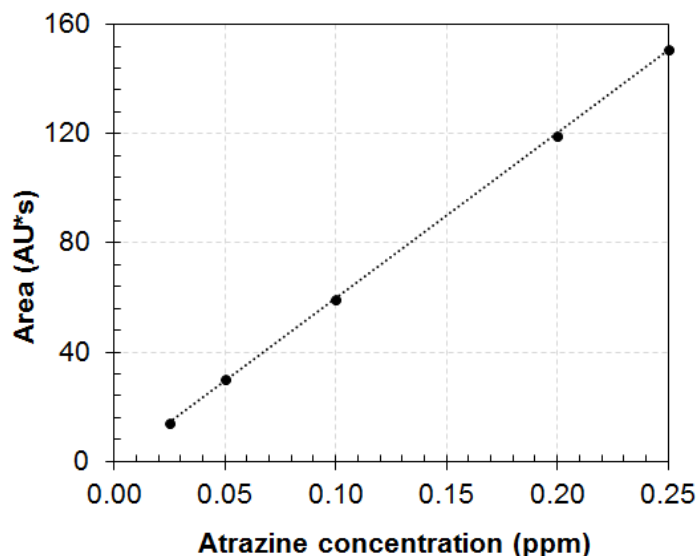


Figure 10: Calibration curve for atrazine concentration in the HPLC unit.

#### 4.3.2 Treatability Studies with TiO<sub>2</sub> in Suspension, UV Light and Glass Substrate Effect

In these treatability studies we evaluated the TiO<sub>2</sub> / glass composite capacity to degrade atrazine solutions. In order to confirm the TiO<sub>2</sub> potential, an initial analysis was completed with the TiO<sub>2</sub> in suspension (i.e. not fixed onto any surface). Figure 10 shows the atrazine levels of a solution in contact with TiO<sub>2</sub> nanoparticles (0.30 g) with and without UV light for 150 minutes. In the graph,  $C_i$  represents the atrazine concentration at any given time and  $C_0$  the initial concentration (0.10 ppm). As shown in Figure 11, no atrazine levels were detected after 120 min under UV light, which indicates apparent complete degradation of atrazine. Without UV light (dark conditions), only 5% of atrazine reduction was observed after 150 min in contact with TiO<sub>2</sub> nanoparticles. This

suggests that TiO<sub>2</sub> nanoparticle has low adsorption capacity of atrazine which suggest weak interactions between atrazine and TiO<sub>2</sub>. [14].

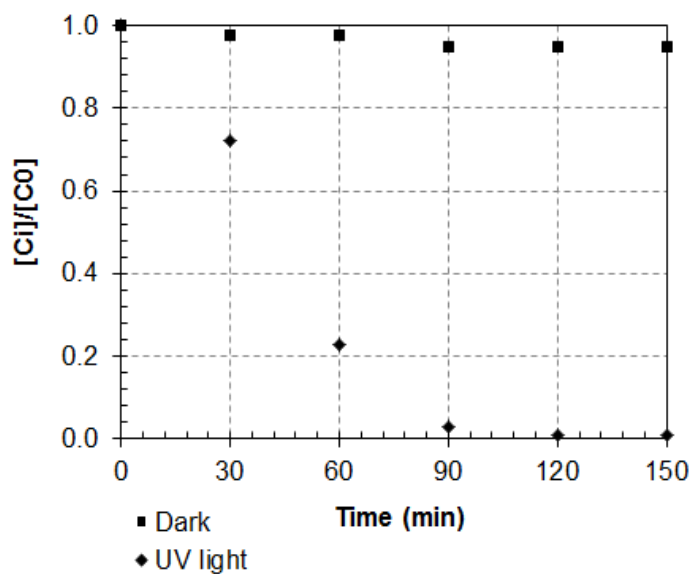


Figure 11: Atrazine levels after TiO<sub>2</sub> time exposure with and without UV light.

The next treatability study consisted of evaluating the UV light effect on the atrazine solution and the adsorption capacity of the glass substrate. Figure 12 shows the atrazine concentrations under UV light and after been in contact with the glass substrate (without TiO<sub>2</sub>) without UV light. There is only a 1% of atrazine concentration drop after 150 min in both analyses, indicating that the 365 nm irradiation not have a significant degradation effect and the whole sintered glass substrate has low adsorption capacity. Others authors have found that the photolytic irradiation that can affect atrazine is near 220 nm [13].

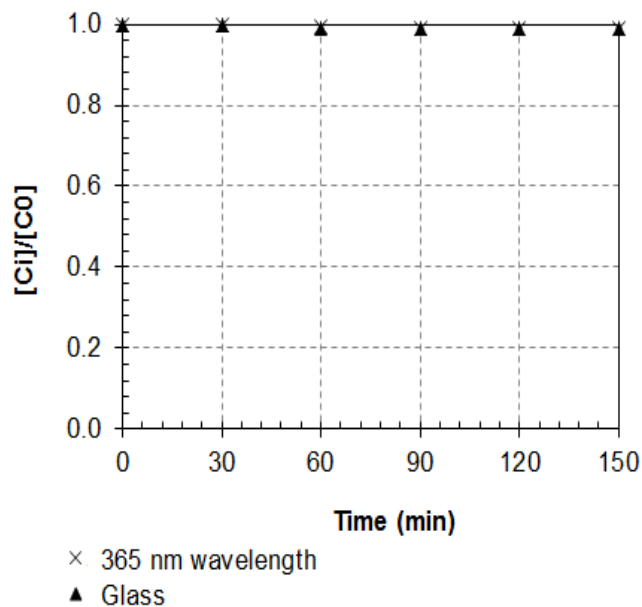


Figure 12: Atrazine levels under UV light and after had been in contact with the glass substrate (without TiO<sub>2</sub>) in the absence of UV light.

#### 4.3.1 Treatability Studies for the TiO<sub>2</sub> / Glass Composite

As stated in the Methodology section, two methods to immobilize/attach the TiO<sub>2</sub> nanoparticles onto the glass substrates were developed and tested for their viability in degrading atrazine solutions under UV light. Figure 13 shows the atrazine concentrations after been in contact with the two types of TiO<sub>2</sub> / glass composite with respect to time. In addition, we deemed important to assess the effect on the atrazine degradation rate of different levels of immobilized TiO<sub>2</sub> (0.30, and 0.50 g). For this analysis, we kept the atrazine concentration constant at 0.10 ppm. Our results revealed a higher degradation rate by the two-layer material than for the combined TiO<sub>2</sub> / glass composite. This suggests that, since the nanoparticles are trapped within the glass

substrate, it was harder for the UV light to reach the immobilized TiO<sub>2</sub> and photo-activate it [3], [45]; hence, the degradation capacity lowered compared to the two-layer composite. Also, the results demonstrate higher degradation capacity with high amounts of TiO<sub>2</sub> in both immobilizing methods, implying more photo-activation site to degrade the contaminant.

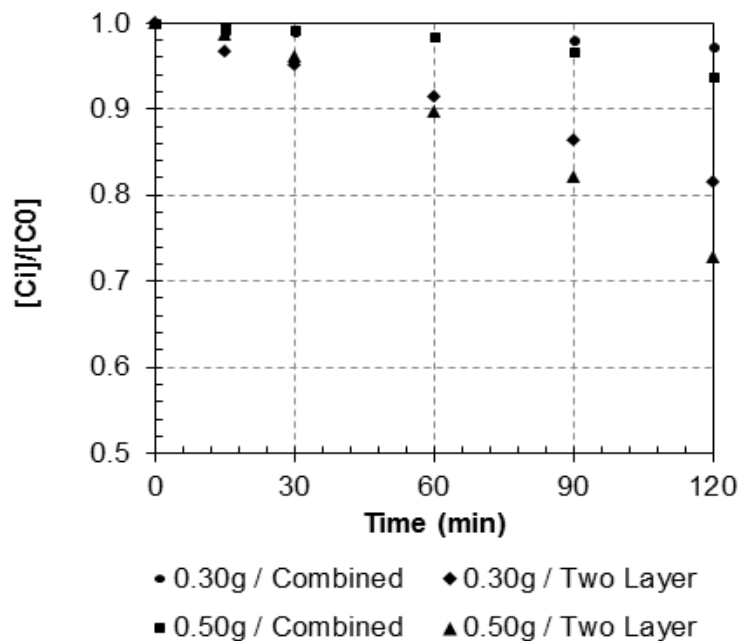


Figure 13: Atrazine levels with time after exposure to the TiO<sub>2</sub> / glass composite under UV light.

Since the TiO<sub>2</sub> deposition technique, denoted by the two-layer TiO<sub>2</sub> / glass composite in Figure 14, acquired the higher atrazine degradation efficiency, further treatability studies with the two-layer TiO<sub>2</sub> / glass composite were conducted varying the TiO<sub>2</sub> mass attached to the glass for a 12 hours of UV light exposure. Figure 13 presents the atrazine degradation percentage in terms of the immobilized TiO<sub>2</sub> amount in the glass composite. An optimum condition was found at 0.55 g of TiO<sub>2</sub> resulting in a 99%



atrazine degradation. Higher amounts of  $\text{TiO}_2$  ( $> 0.55\text{g}$ ) do not improve the degradation of atrazine, as shown in Figure 13. This could be attributed to the overlapping of  $\text{TiO}_2$  layers, which can limit the active surface area by the increment in particle size [22], [46].

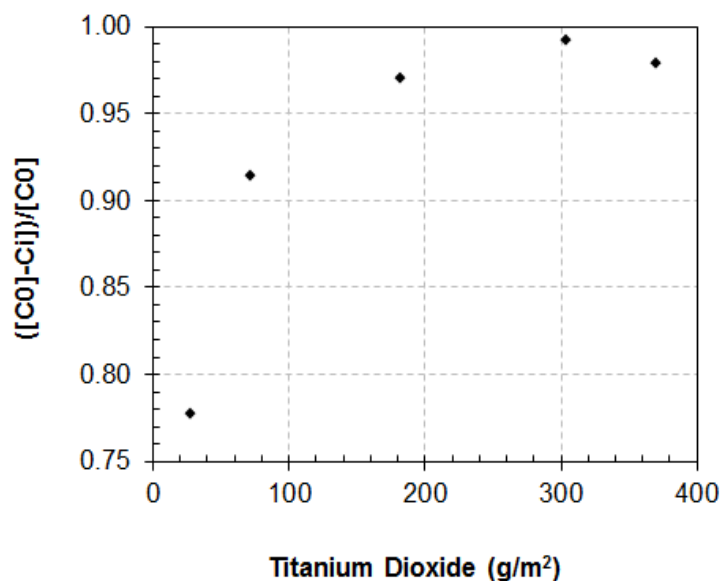


Figure 14: Atrazine degradation (%) per mass of  $\text{TiO}_2$  immobilized on the two-layer  $\text{TiO}_2$  / glass composite.

#### 4.3.2 Treatability Studies for Variable Atrazine Concentrations

The degradation capacity of the  $\text{TiO}_2$  / glass composite was also verified at various atrazine concentrations. An experimental set was designed to run three different atrazine concentrations (0.050, 0.100 and 0.250 ppm) in contact with 0.33 g of immobilized  $\text{TiO}_2$  (two-layer  $\text{TiO}_2$  / glass composite) for 12 hours under UV light. Figure

15 presents the atrazine concentration as a function of time for each evaluated atrazine dilution. According to the data obtained, the lower the initial atrazine concentration, the higher the degradation rate.

In addition, the kinetic reaction of the atrazine degradation seems to follow a pseudo-first order where the initial concentration of the contaminant has strong effect in the degradation capacity. Table 6 shows the degradation rate constant of atrazine at each studied condition obtained by a linear relationship of the plot  $\ln C_0$  versus time (Appendix B). Our results revealed that higher concentration levels reduced the available active sites to degrade the contaminant [47], [48], which reduced the efficiency as denoted by a lower value of the degradation rate constant.

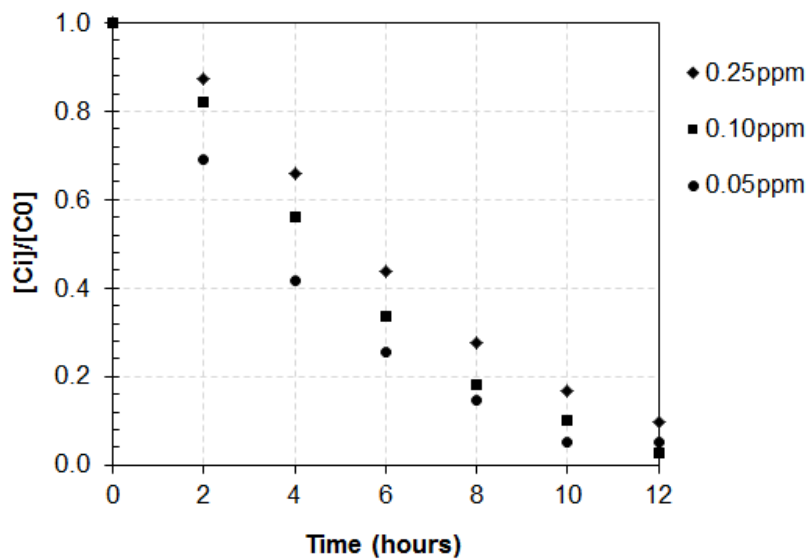


Figure 15: Atrazine levels for variable concentrations in contact with the  $\text{TiO}_2$  / glass composite under UV light

Table 6: Degradation rate constant for three different concentrations of atrazine

Atrazine concentration (ppm)	Degradation Rate of Constant (1/h)	R <sup>2</sup>
0.050	0.285	0.968
0.100	0.235	0.974
0.250	0.184	0.966

#### 4.3.3 Treatability Studies at Different Nanoparticles Size

The atrazine degradation rate can be affected by the TiO<sub>2</sub> particle size. In order to evaluate this effect, we conducted a treatability study using two different particle sizes of TiO<sub>2</sub> immobilized onto the glass substrate (two-layer TiO<sub>2</sub> / glass composite). The nanoparticles size was determined using XRD analysis and Scherrer's equation, i.e. Eq. 1 (Appendix A part c), which estimated particle sizes of 16 and 32 nm of the anatase polymorph.

The treatability studies were performed immobilizing 0.33 g of each nanoparticle size specimen onto two different glass substrates. Each resulting TiO<sub>2</sub> / glass composite (with TiO<sub>2</sub> particle sizes of 16 and 32 nm each) were placed in contact with a 0.10 ppm atrazine solution. Figure 16 shows the atrazine reduction after 12 hours under UV light. Also, Table 7 presents the degradation rate constant obtained for each particle size. These results suggest that higher degradation rates were attained with smaller particle size, i.e. 16 nm, which in agreement with the literature [22]. In effect, the active surface

area is higher for the small nanoparticle size [43] and, thus, more free radicals were able to degrade the contaminant.

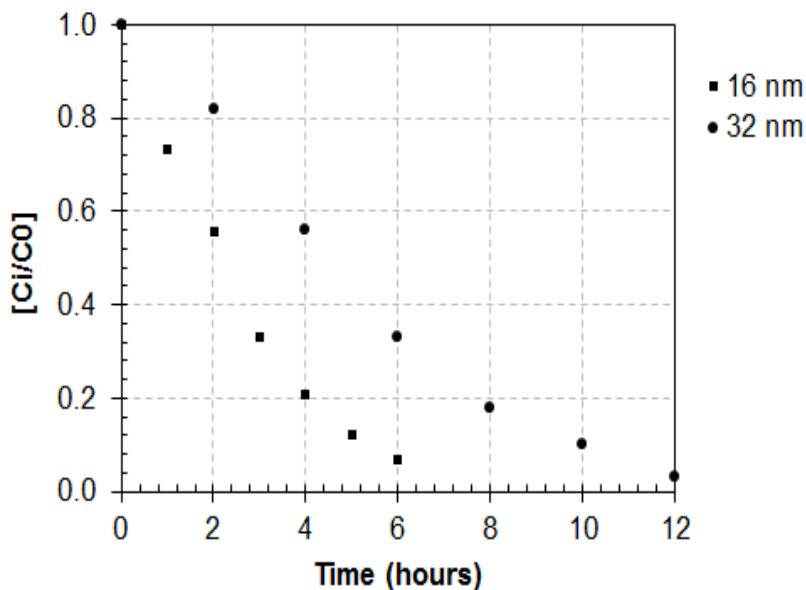


Figure 16: Atrazine levels with the TiO<sub>2</sub> / glass composite embedded with a certain TiO<sub>2</sub> nanoparticle size.

Table 7: Degradation rate constant for different TiO<sub>2</sub> particle sizes.

TiO <sub>2</sub> particle size (nm)	Degradation Rate Coefficient (1/h)	R <sup>2</sup>
16	0.426	0.984
32	0.237	0.974

In order to identify the exhaustion point of the TiO<sub>2</sub> / glass composite, multiple batches of fresh atrazine were used keeping the same TiO<sub>2</sub> / glass composite. The experiment was performed for three continuous batches during 12 h of UV light

exposure each, for a total run of 36 h. At the end of each batch, i.e. 12 h, the atrazine dilution was replaced by a newly fresh one of 0.10 ppm. Figure 17 presents the atrazine concentration with time for each batch. As shown, the degradation capacity of the  $\text{TiO}_2$  / glass composite decreases at the end of the third batch, i.e. after 36 h of use, as the residual atrazine levels is higher than in the previous two batches. This effectiveness decrease can be quantified as a 3% degradation capacity reduction. In comparison with other similar studies, this composite presents an extended useful live [22].

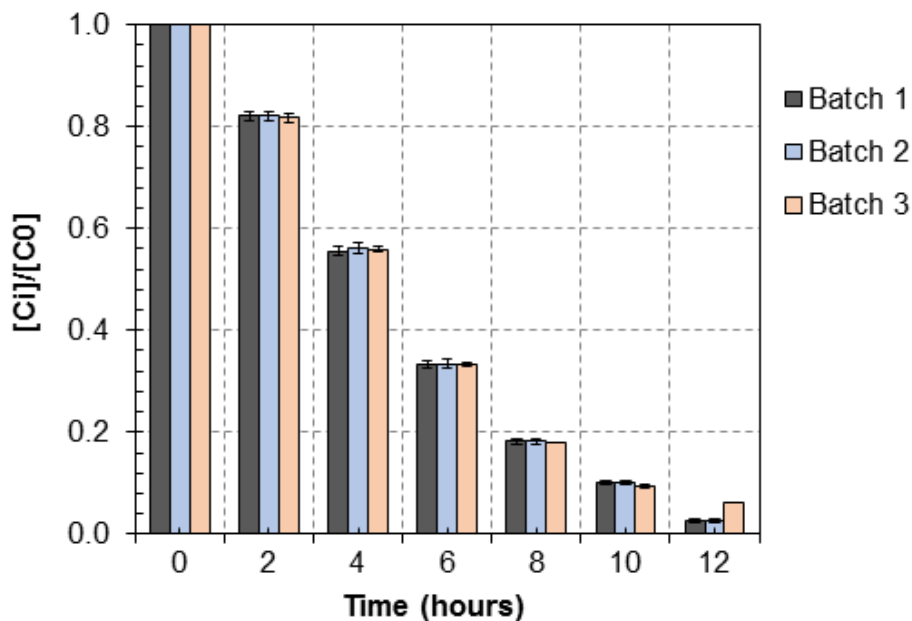


Figure 17: Atrazine levels conducted in three different batches (12 hours each) for a single  $\text{TiO}_2$  / glass composite exposed to UV light.

#### 4.4 Percolation Rate

The percolation experiments were carried out to study the capacity of the material to permit water circulation through the porous composite. The percolation rate is expressed as a water flux (water flow per composite surface area) with unit dimensions of  $\text{m}^3/\text{s}\cdot\text{m}^2$ . (A constant diameter of 1.90 inches was kept for all evaluated composites).

In this research segment, we first prepared the glass substrates by sintering crushed glass particles at 950 °C, 963 °C and 775 °C for 45 min, 60 min, and 75 min. Figure 18 presents the percolation rate average measured at each sintering condition.

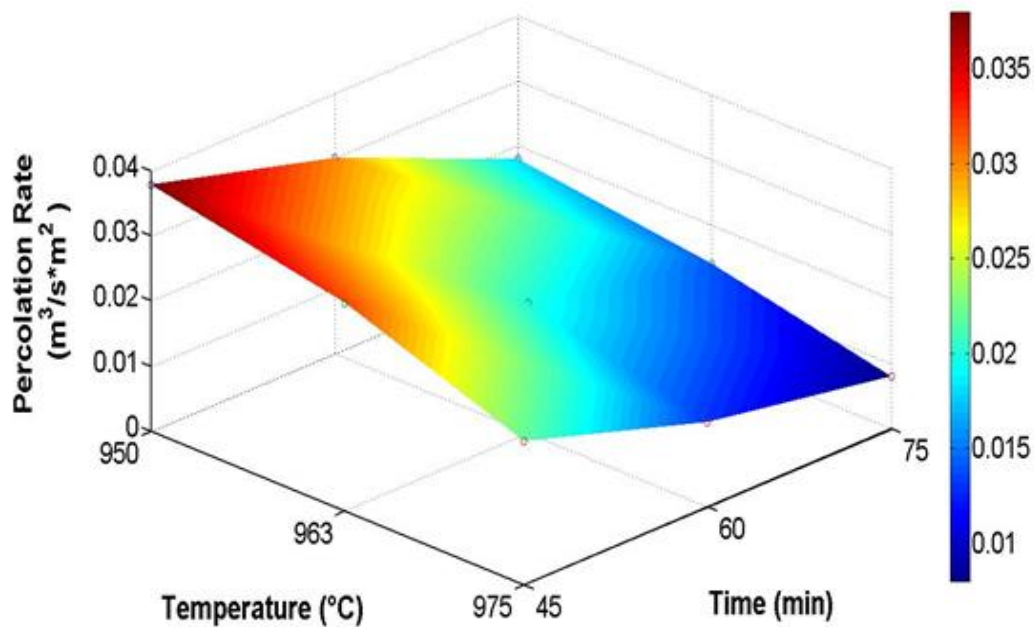


Figure 18: Performance map of percolation rate for the sintered glass substrates in ( $\text{m}^3/\text{s}\cdot\text{m}^2$ ) as function of the sintering temperature and time.

Then, a percolation rate was performed for the two-layer TiO<sub>2</sub> / glass composite with approximately 0.33 g of TiO<sub>2</sub> immobilized using a water/ethanol/TiO<sub>2</sub> suspension and heat treated at 900°C for 2 hours. Figure 19 shows the average of the results of the material sintered at 950 °C, 963 °C and 775 °C for 45 min, 60 min, and 75 min. The highest percolation rate was observed for a filter sintered at 950 °C for 45 min: 0.038 and 0.023 m<sup>3</sup>/s-m<sup>2</sup> for the glass only substrate and the TiO<sub>2</sub> / glass composite, respectively. In both figures (Fig 18 and 19) one can observe that the percolation rate decreases for higher sintering temperature and longer sintering time. This is natural since increasing times facilitates viscous flows and, consequently, densification mechanisms that shrinks the pores. Also, increasing sintering temperature allows further pore shrinking by providing more energy for the system's solid state and partial liquid sintering mechanisms (surface and volume diffusion), which lowers the percolation rates [49].

Table 8 presents a comparison of the percolation rates acquired for both the whole glass substrates (without TiO<sub>2</sub>) and the TiO<sub>2</sub> / glass composite material. According to these data, one can observe that the percolation rate through the glass substrates is adversely affected by the addition of the TiO<sub>2</sub> nanoparticles when compared with the results from the glass filters without TiO<sub>2</sub>. The nanoparticles block the glass sintered porous resulting in a reduction of the percolation rate.

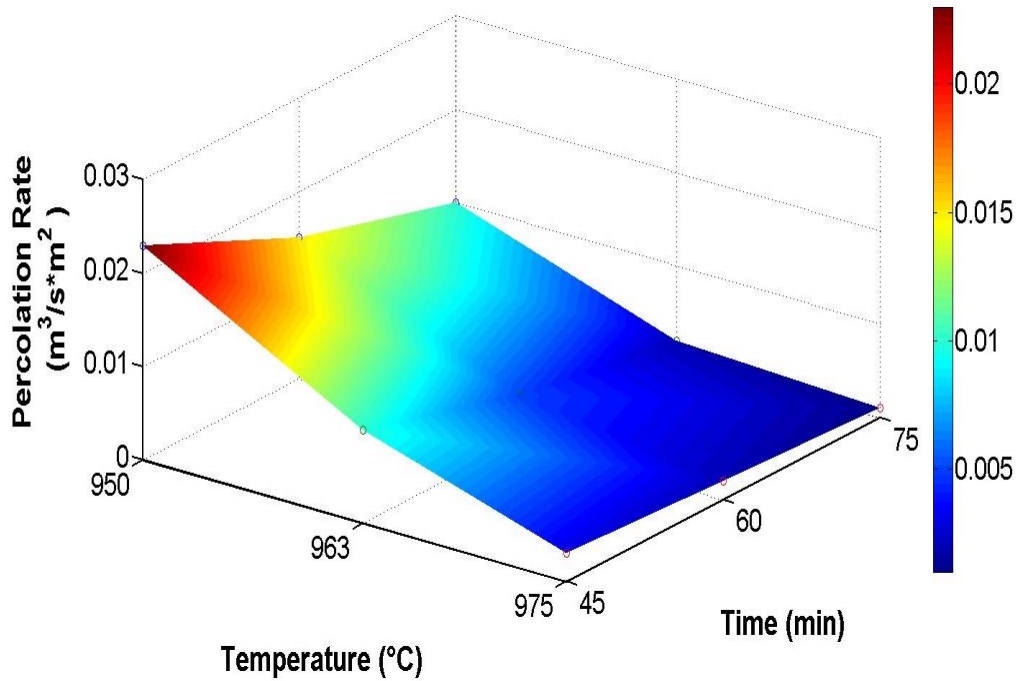


Figure 19: Performance map of percolation rate for the sintered TiO<sub>2</sub>/ glass composite in (m<sup>3</sup>/s·m<sup>2</sup>) as a function of sintering temperature and time.

Table 8: Comparison of percolation rates for the glass filter and TiO<sub>2</sub> / glass composite material for the studied sintered parameters.

Time (min)	950°C			963°C			975°C		
	Glass	TiO <sub>2</sub> / Glass	% Red	Glass	TiO <sub>2</sub> / Glass	% Red	Glass	TiO <sub>2</sub> / Glass	% Red
45	0.038	0.023	39.30	0.032	0.010	69.91	0.022	0.003	85.09
60	0.030	0.015	50.33	0.020	0.005	77.56	0.013	0.002	84.60
75	0.018	0.010	46.93	0.014	0.002	88.39	0.008	0.001	86.68



## 4.5 Compressive Strength Analysis

In this research segment, we measured the compressive strength of the porous materials to determine the maximum load they may sustain before breaking. Figure 20 shows the relationship between the glass substrate fracture strength in MPa as a function of the sintering parameters. Naturally, an increase in the sintering time and temperature caused higher values for compression strength since longer times or higher temperatures allow faster densification that shrinks the porosity of the material. Less flaws correlates to a lower probability of crack formation which in turn higher the fracture strength [50].

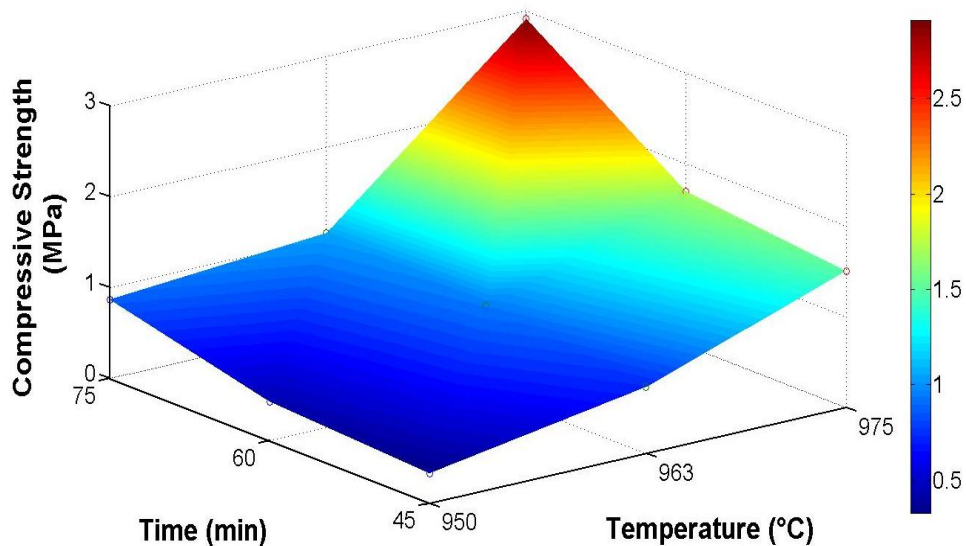


Figure 20: Performance map for the glass compressive strength as function of sintering temperature and time.

## 5 Potential Application

The principal source of the herbicides are the agriculture sites, which by the action of the precipitation (run off) are causing the contamination of the surface water as rivers and lakes. An alternative to degrade this contaminant can be a glass substrate embedded with TiO<sub>2</sub> nanoparticles developed in this research.

The ultimate goal of the TiO<sub>2</sub> / glass composite would be its implementation in storm drainage system or run off channels in agriculture sites before the contaminant reaches a surface water source. Degradation can occur by the contact of the contaminant water with the TiO<sub>2</sub> nanoparticles, which under the UV light of the sun, degrades the contaminant by a photocatalytic reaction. To extend the contact time of the contaminant with the nanoparticles a waterfall of TiO<sub>2</sub> / glass composite can be developed.

## 6 Recomendations

- Study the degradation capacity of other herbicides employing the TiO<sub>2</sub> / glass composite material developed by this research.
- Study the implementation of the TiO<sub>2</sub> / glass composite under uncontrolled (real life) conditions.

## 7 Conclusions

The indiscriminate use of herbicides has caused the contamination of water bodies (surface or groundwater) with toxic organic compounds. Advance oxidation process emerges as an alternative to degrade these types of contaminants. This can be achieved by using a catalytic material, such as  $\text{TiO}_2$ , which can be photo-activated under the influence of UV-light.

Two different techniques were developed and evaluated in this research for the immobilization of  $\text{TiO}_2$  within a sintered, recycled glass substrate for the degradation of atrazine, one of the most used herbicide in U.S. The immobilization technique consisting in sintering together the  $\text{TiO}_2$  nanoparticles with the glass particles showed effective immobilization capacity. However, very low photo-degradation levels of atrazine were attained (less than 10% degradation).

The immobilization approach consisting of the gravitational deposition and heating retained lower  $\text{TiO}_2$  nanoparticles when compared to the combined method. Nevertheless, it achieved higher degradation capacity for destroying atrazine than in the combined approach (99% degradation). This suggests that the  $\text{TiO}_2$  nanoparticles fixed onto the glass surface had more access to the UV light, hence, higher photo-activation capacity than in the combined composite.

Finally, an inverse relationship was observed between the percolation rate and the sintering parameters (temperature and time) for the glass substrate and the two-layer  $\text{TiO}_2$  / glass composite. Conversely, the filters compressive strength was higher for longer sintering times and temperatures.

## 8 References

- [1] W. Bahnemann, M. Muneer, and M. M. Haque, "Titanium dioxide-mediated photocatalysed degradation of few selected organic pollutants in aqueous suspensions," *Catal. Today*, vol. 124, no. 3–4, pp. 133–148, 2007.
- [2] W. W. Stone, R. J. Giliom, and J. D. Martin, "An Overview Comparing Results from Two Decades of Monitoring for Pesticides in the Nation's Streams and Rivers, 1992–2001 and 2002–2011," Reston, Virginia, USA, 2014.
- [3] S. Leong, A. Razmjou, K. Wang, K. Hapgood, X. Zhang, and H. Wang, "TiO<sub>2</sub> based photocatalytic membranes: A review," *J. Memb. Sci.*, vol. 472, pp. 167–184, 2014.
- [4] M. O. Ribaudó and A. Bouzaher, "Atrazine : Environmental Characteristics and Economics of Management," 1994.
- [5] Agency for Toxic Substance and Disease Registry, "ToxGuide for Atrazine," 2003.
- [6] Z. Liu, Y. Wang, Z. Zhu, E. Yang, X. Feng, Z. Fu, and Y. Jin, "Chemosphere Atrazine and its main metabolites alter the locomotor activity of larval zebrafish (*Danio rerio*)," *Chemosphere*, vol. 148, pp. 163–170, 2016.
- [7] B. Prado, C. Duwig, C. Hidalgo, K. Müller, L. Mora, E. Raymundo, and J. D. Etchevers, "Transport, sorption and degradation of atrazine in two clay soils from Mexico: Andosol and Vertisol," *Geoderma*, vol. 232–234, pp. 628–639, 2014.
- [8] G. Zhanqi, Y. Shaogui, T. Na, and S. Cheng, "Microwave assisted rapid and complete degradation of atrazine using TiO<sub>2</sub> nanotube photocatalyst suspensions," *J. Hazard. Mater.*, vol. 145, no. 3, pp. 424–430, 2007.
- [9] M. B. Murphy, M. Hecker, K. K. Coady, A. R. Tompsett, P. D. Jones, L. H. Du Preez, G. J. Everson, K. R. Solomon, J. A. Carr, E. E. Smith, R. J. Kendall, G. Van Der Kraak, and J. P. Giesy, "Atrazine concentrations, gonadal gross morphology and histology in ranid frogs collected in Michigan agricultural areas," *Aquat. Toxicol.*, vol. 76, pp. 230–245, 2006.
- [10] S. Papoutsakis, Z. Afshari, S. Malato, and C. Pulgarin, "Journal of Environmental Chemical Engineering Elimination of the iodinated contrast agent iohexol in water, wastewater and urine matrices by application of photo-Fenton and ultrasound advanced oxidation processes," *Biochem. Pharmacol.*, 2015.
- [11] H. Suzuki, S. Araki, and H. Yamamoto, "Journal of Water Process Engineering Evaluation of advanced oxidation processes ( AOP ) using O<sub>3</sub> , UV , and TiO<sub>2</sub> for the degradation of phenol in water," *J. Water Process Eng.*, vol. 7, pp. 54–60, 2015.

- [12] D. A. H. Hanaor and C. C. Sorrell, "Review of the anatase to rutile phase transformation," *J. Mater. Sci.*, vol. 46, pp. 855–874, 2011.
- [13] V. Héquet, C. Gonzalez, and P. Le Cloirec, "Photochemical processes for atrazine degradation: Methodological approach," *Water Res.*, vol. 35, no. 18, pp. 4253–4260, 2001.
- [14] S. Parra, S. E. Stanca, I. Guasaquillo, and K. Ravindranathan Thampi, "Photocatalytic degradation of atrazine using suspended and supported TiO<sub>2</sub>," *Appl. Catal. B Environ.*, vol. 51, no. 2, pp. 107–116, 2004.
- [15] P. Lei, F. Wang, X. Gao, Y. Ding, S. Zhang, J. Zhao, S. Liu, and M. Yang, "Immobilization of TiO<sub>2</sub> nanoparticles in polymeric substrates by chemical bonding for multi-cycle photodegradation of organic pollutants," *J. Hazard. Mater.*, vol. 227–228, pp. 185–194, 2012.
- [16] K. Huang, A. M. Grumezescu, C. Chang, C. Yang, and C. Wang, "Immobilization and stabilization of TiO<sub>2</sub> nanoparticles in Alkaline-solidificated chitosan speres without cross-linking agent," *Int. J. Latest Res. Sci. Technol.*, vol. 3, no. 2, 2014.
- [17] S. Singh, P. K. Singh, and H. Mahalingam, "A novel and effective strewn polymer-supported titanium dioxide photocatalyst for environmental remediation," *J. Mater. Environ. Sci.*, vol. 6, no. 2, pp. 349–358, 2015.
- [18] G. Kenanakis and N. Katsarakis, "Journal of Environmental Chemical Engineering Chemically grown TiO<sub>2</sub> on glass with superior photocatalytic properties," *Biochem. Pharmacol.*, vol. 2, pp. 1748–1755, 2014.
- [19] T. Zhang, Y. Luo, B. Jia, Y. Li, L. Yuan, and J. Yu, "Immobilization of self-assembled pre-dispersed nano- TiO<sub>2</sub> onto montmorillonite and its photocatalytic activity," *J. Environ. Sci. (China)*, vol. 32, pp. 108–117, 2015.
- [20] R. S. Sonawane, S. G. Hegde, and M. K. Dongare, "Preparation of titanium(IV) oxide thin film photocatalyst by sol-gel dip coating," *Mater. Chem. Phys.*, vol. 77, no. 3, pp. 744–750, 2003.
- [21] S. Vyas, R. Tiwary, K. Shubham, and P. Chakrabarti, "Study the target effect on the structural, surface and optical properties of TiO<sub>2</sub> thin film fabricated by RF sputtering method," *Superlattices Microstruct.*, vol. 80, pp. 215–221, 2015.
- [22] M. L. Yola, T. Eren, and N. Atar, "A novel efficient photocatalyst based on TiO<sub>2</sub> nanoparticles involved boron enrichment waste for photocatalytic degradation of atrazine," *Chem. Eng. J.*, vol. 250, pp. 288–294, 2014.
- [23] O. Sacco, V. Vaiano, C. Han, D. Sannino, and D. D. Dionysiou, "Photocatalytic removal of atrazine using N-doped TiO<sub>2</sub> supported on phosphors," *Appl. Catal. B Environ.*, vol. 164, pp. 462–474, 2015.

- [24] K. P. Singh, A. Malik, and S. Sinha, "Water quality assessment and apportionment of pollution sources of Gomti river (India) using multivariate statistical techniques - A case study," *Anal. Chim. Acta*, vol. 538, no. 1–2, pp. 355–374, 2005.
- [25] P. Hecq, A. Hulsmann, F. S. Hauchman, J. L. Mclain, and F. Schmitz, *Drinking Water Regulations*. 2005.
- [26] EPA, "Priority Pollutant List," pp. 1–2, 2014.
- [27] C. Fedtke and S. O. Duke, "Herbicides," no. 3, 2005, pp. 1–84.
- [28] E. H. Smith and G. G. Kennedy, "History of pesticides," *Encyclopedia of Pest Management*. pp. 376–380, 2002.
- [29] EPA, "National Primary Drinking Water Regulations," *EPA 816-F-09-004*, pp. 1–6, 2009.
- [30] G. Xu, T. Bu, M. Wu, J. Zheng, N. Liu, and L. Wang, "Electron beam induced degradation of clopyralid in aqueous solutions," *J. Radioanal. Nucl. Chem.*, vol. 288, no. 3, pp. 759–764, 2011.
- [31] M. Graymore, F. Stagnitti, and G. Allinson, "Impacts of atrazine in aquatic ecosystems," *Environ. Int.*, vol. 26, pp. 483–495, 2001.
- [32] J. A. Santacruz-Chavez, S. Oros-Ruiz, B. Prado, and R. Zanella, "Photocatalytic degradation of atrazine using TiO<sub>2</sub> superficially modified with metallic nanoparticles," *J. Environ. Chem. Eng.*, 2015.
- [33] F. E. Dayan, S. O. Duke, and K. Grossmann, "Herbicides as Probes in Plant Biology," *Weed Sci.*, vol. 58, pp. 340–350, 2010.
- [34] C. Luo, J. Ma, J. Jiang, Y. Liu, Y. Song, Y. Yang, Y. Guan, and D. Wu, "Simulation and comparative study on the oxidation kinetics of atrazine by UV/H<sub>2</sub>O<sub>2</sub>," *Water Res.*, vol. 80, pp. 99–108, 2015.
- [35] "Special issue on 'Environmental applications of advanced oxidation processes,'" *Hazard. Mater.*, vol. 146, p. 439, 2007.
- [36] B. Bhaskar, S. H. Sonawane, B. A. Bhanvase, and S. Gumfekar, "Nanomaterials based Advanced Oxidation Processes for Waste Water Treatment: A review," *Chem. Eng. Process. Process Intensif.*, vol. 109, pp. 178–189, 2016.
- [37] A. Karci, "Degradation of chlorophenols and alkylphenol ethoxylates, two representative textile chemicals, in water by advanced oxidation processes: The state of the art on transformation products and toxicity," *Chemosphere*, vol. 99, pp. 1–18, 2014.

- [38] K. Hashimoto, H. Irie, and A. Fujishima, "TiO<sub>2</sub> Photocatalysis: A Historical Overview and Future Prospects," *Jpn. J. Appl. Phys.*, vol. 44, no. 12, pp. 8269–8285, 2005.
- [39] M. L. Yola, T. Eren, and N. Atar, "A novel efficient photocatalyst based on TiO<sub>2</sub> nanoparticles involved boron enrichment waste for photocatalytic degradation of atrazine," vol. 250, pp. 288–294, 2014.
- [40] W. Cuadrado, "Fabrication and Characterization of Sintered Recycled Glass Designed for Polluted Soil Filtering," University of Puerto Rico, Mayaguez Campus, 2014.
- [41] C. B. Carter and M. G. Norton, *Ceramic Materials Science and Engineering*. 2013.
- [42] M. N. Rahaman, *Sintering of Ceramics*. 2008.
- [43] N. Xu, Z. Shi, Y. Fan, J. Dong, J. Shi, and M. Z. Hu, "Effects of Particle Size of TiO<sub>2</sub> on Photocatalytic Degradation of Methylene Blue in Aqueous Suspensions," *Ind. Eng. Chem. Res.*, pp. 373–379, 1999.
- [44] A. Sclafani and J. M. Herrmann, "Comparison of the Photoelectronic and Photocatalytic Activities of Various Anatase and Rutile Forms of Titania in Pure Liquid Organic Phases and in Aqueous Solutions," *J. Phys. Chem.*, vol. 100, no. i, pp. 13655–13661, 1996.
- [45] S. H. Othman, S. Abdul Rashid, T. I. Mohd Ghazi, and N. Abdullah, "Dispersion and stabilization of photocatalytic TiO<sub>2</sub> nanoparticles in aqueous suspension for coatings applications," *J. Nanomater.*, vol. 2012, 2012.
- [46] S. Parra, S. Elena Stanca, I. Guasaquillo, and K. Ravindranathan Thampi, "Photocatalytic degradation of atrazine using suspended and supported TiO<sub>2</sub>," *Appl. Catal. B Environ.*, vol. 51, no. 2, pp. 107–116, Jul. 2004.
- [47] S. Alahiane, S. Qourzal, M. El Ouardi, A. Abamrane, and A. Assabbane, "Factors Influencing the Photocatalytic Degradation of Reactive Yellow 145 by TiO<sub>2</sub>-Coated Non-Woven Fibers," *Am. J. Anal. Chem.*, vol. 5, no. June, pp. 445–454, 2014.
- [48] C. Chiou and R. Juang, "Photocatalytic degradation of phenol in aqueous solutions by Pr-doped TiO<sub>2</sub> nanoparticles," *J. Hazard. Mater.*, vol. 149, pp. 1–7, 2007.
- [49] D. Yang, Y. Zhang, X. Song, Y. Chen, Z. Shen, and C. Yang, "Effects of sintering temperature and holding time on porosity and shrinkage of glass tubes," *Ceram. Int.*, vol. 42, no. 5, pp. 5906–5910, 2016.

- [50] L. Hu and C.-A. Wang, "Effect of sintering temperature on compressive strength of porous yttria-stabilized zirconia ceramics," *Ceram. Int.*, vol. 36, no. 5, pp. 1697–1701, 2010.



## Appendix A: Determination fo the settling velocity of the TiO<sub>2</sub> nanoparticles in suspension

Settling velocity stated by Stokes' law for a discrete particle was implemented to study the gravitational deposition of the TiO<sub>2</sub> nanoparticles employing two different solvents ethanol and acetic acid in water. The equation used was defined as:

$$V_s = \frac{g}{18\mu} (\rho_s - \rho)d_p^2 \quad [1]$$

where, g is the gravitational constant (9.8 m/s<sup>2</sup>); μ is the viscosity of the suspension (kg/m-s); ρ<sub>s</sub> is the density of the particle (kg/m<sup>3</sup>); ρ is the density of the suspension (kg/m<sup>3</sup>); and d<sub>p</sub> is the diameter of the particle (m). To calculate the settling velocity the parameters as the viscosity of the suspension, the diameter of the particle and the density of the suspension were measured experimentally. The Table 1 presents the obtained values.

Table 1: Experimental parameters of the suspension in the gravitational deposition

Solvents	Density of Suspension (kg/m <sup>3</sup> )	Viscosity of Suspension (kg/m-s)	Particle Size in suspension (nm)
Ethanol	905.8	0.0017	365
Acetic Acid	986.7	0.0013	729

The equations 1 was used to calculate the settling velocity for TiO<sub>2</sub> nanoparticles in ethanol/water suspension employing the experimental values and considering some

constant parameters show in Table 2. Also, a Reynolds number were calculated to verify that the equation can be implemented for the developed suspension ( $R_d < 1$ ).

Table 2: Constant parameters of settling velocity equation

Parameters	Values
Viscosity Constant -K (cSt/s)	0.03
Gravity Constant (m/s <sup>2</sup> )	9.81
Density of TiO <sub>2</sub> particle (g/cm <sup>3</sup> )	4.23

Example of calculation:

$$V_s = \frac{g}{18\mu} (\rho_s - \rho) d_p^2$$

$$V_s = \left( \frac{\frac{9.8m}{s^2}}{18 \left( \frac{0.0017kg}{m * s} \right)} \right) \left( \frac{4230kg}{m^3} - \frac{905.8kg}{m^3} \right) (3.65 * 10^{-7}m)^2$$

$$V_s = 0.144 * 10^{-7}m = \frac{0.144\mu m}{s}$$

$$Reynolds = \frac{\rho V_s d}{\mu}$$

$$Reynolds = \frac{\left( \frac{905.8kg}{m^3} \right) (0.144 * 10^{-7}m) (3.65 * 10^{-7}m)}{\frac{0.0017kg}{m * s}} = 2.85 * 10^{-8}$$

## Appendix B: Characterization of TiO<sub>2</sub> nanoparticles by XRD analysis

### A. TiO<sub>2</sub> immobilized by heat treatment onto the surface of the sintered glass

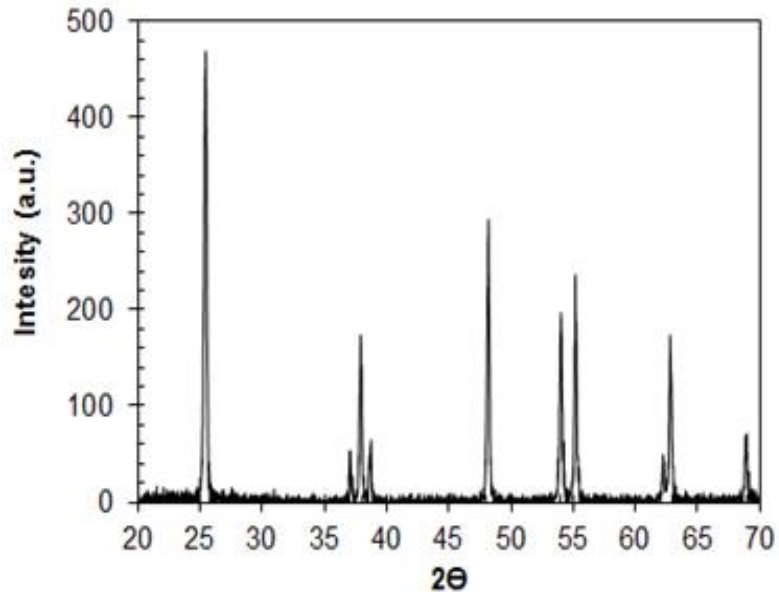


Figure 1: XRD diffractogram for two-layer glass-TiO<sub>2</sub> composite performed with water/acetic acid suspension and exposed at 600°C for 2 hours of heat treatment.

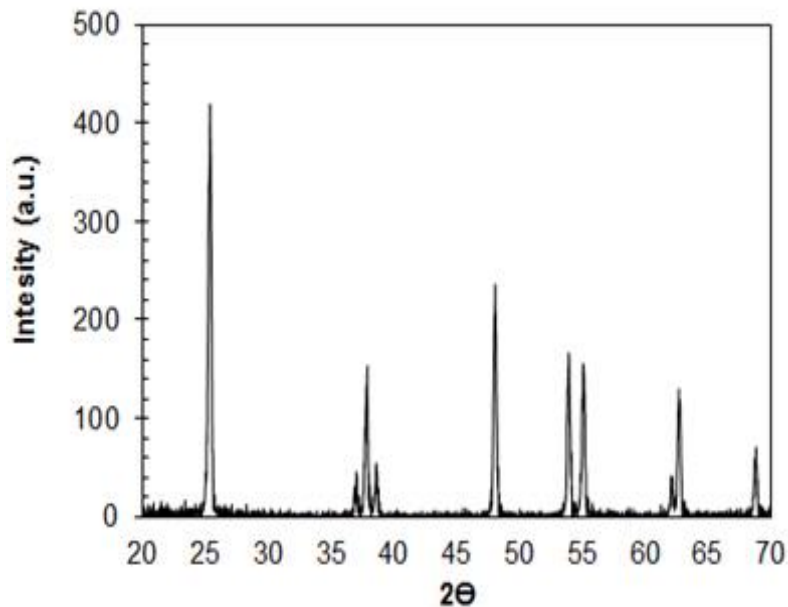


Figure 2: XRD diffractogram for two-layer glass-TiO<sub>2</sub> composite performed with water/acetic acid suspension and exposed at 600°C for 4 hours of heat treatment.

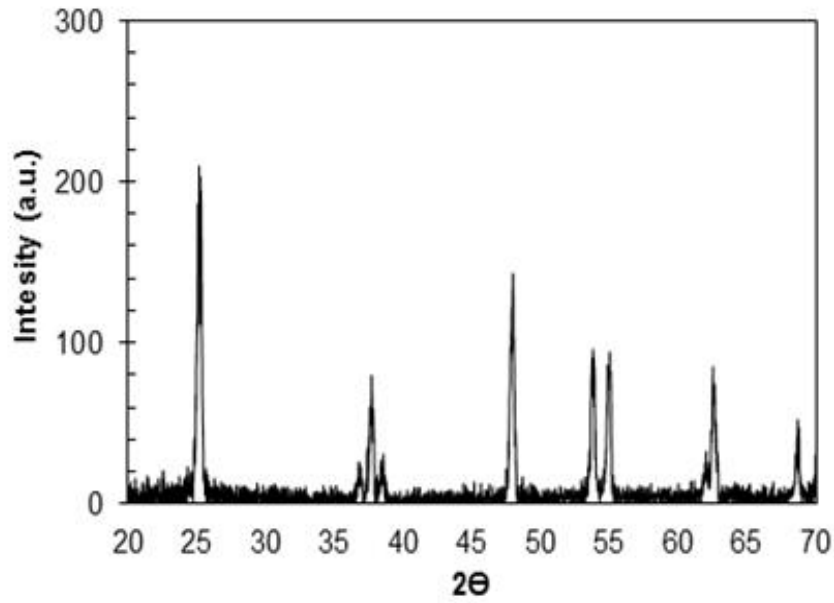


Figure 3: XRD diffractogram for two-layer glass-TiO<sub>2</sub> composite performed with water/acetic acid suspension and exposed at 900°C for 2 hours of heat treatment.

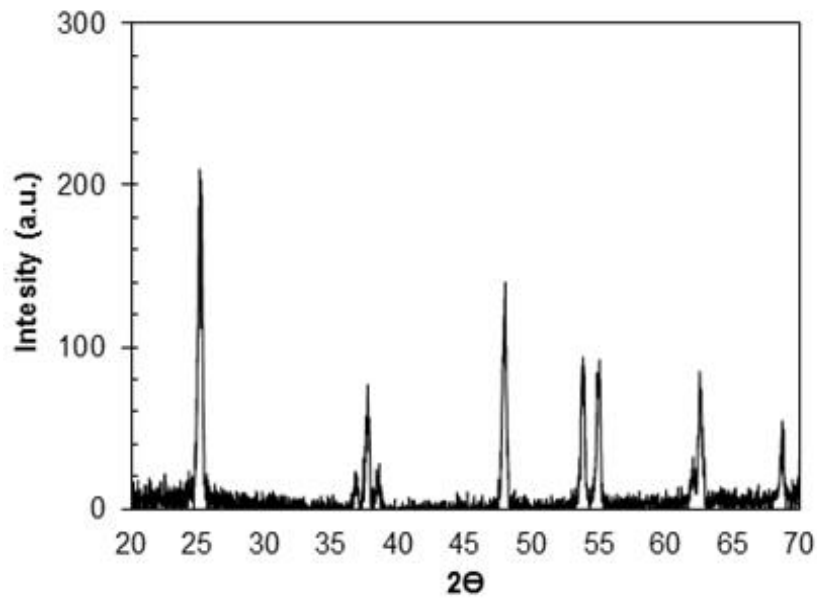


Figure 4: XRD diffractogram for two-layer glass-TiO<sub>2</sub> composite performed with water/acetic acid suspension and exposed at 900°C for 4 hours of heat treatment.

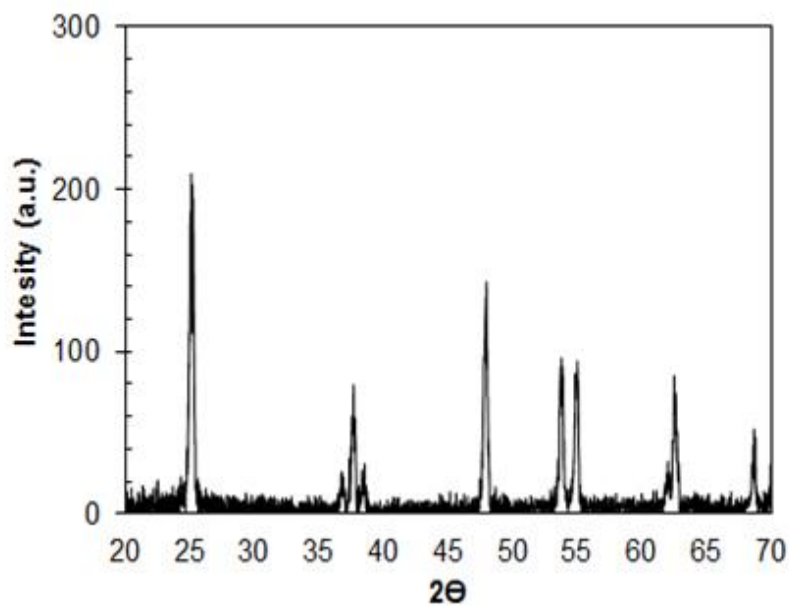


Figure 5: XRD diffractogram for two-layer glass-TiO<sub>2</sub> composite performed with water/ethanol suspension and exposed at 600°C for 2 hours of heat treatment.

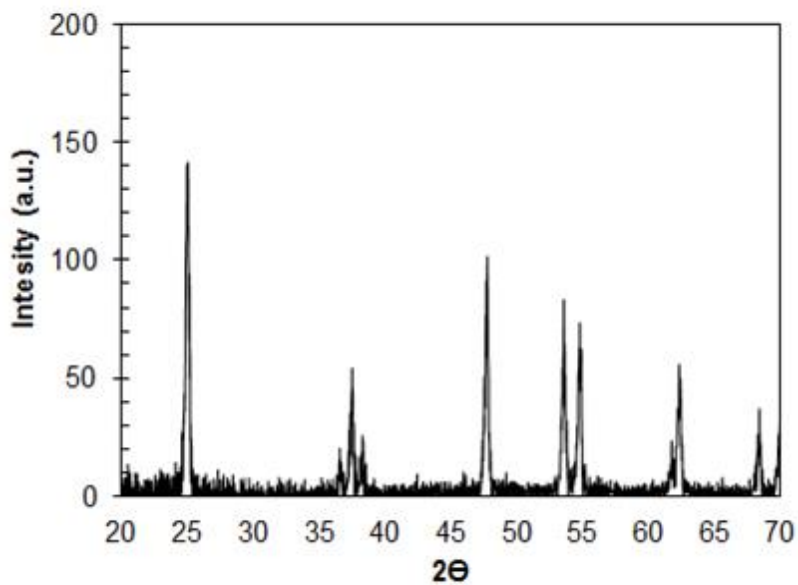


Figure 6: XRD diffractogram for two-layer glass-TiO<sub>2</sub> composite performed with water/ethanol suspension and exposed at 600°C for 4 hours of heat treatment.

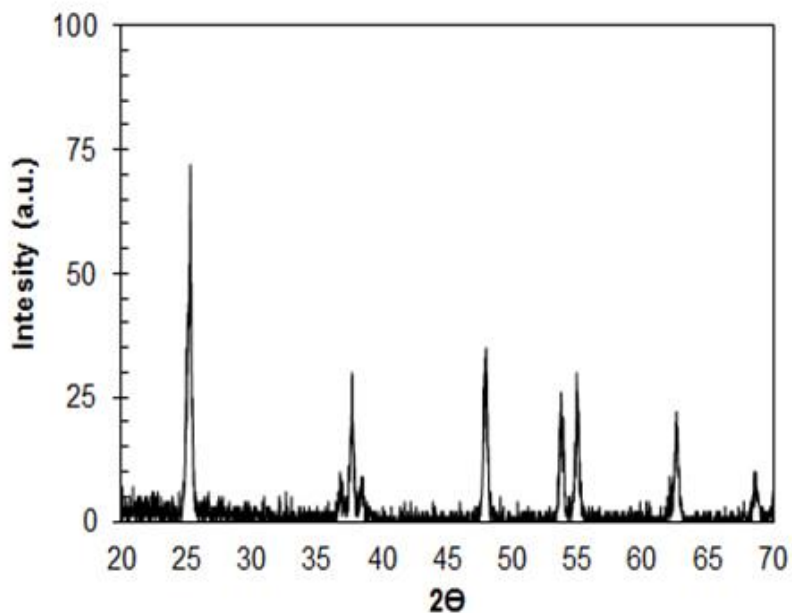


Figure 7: XRD diffractogram for two-layer glass-TiO<sub>2</sub> composite performed with water/ethanol suspension and exposed at 900°C for 2 hours of heat treatment.

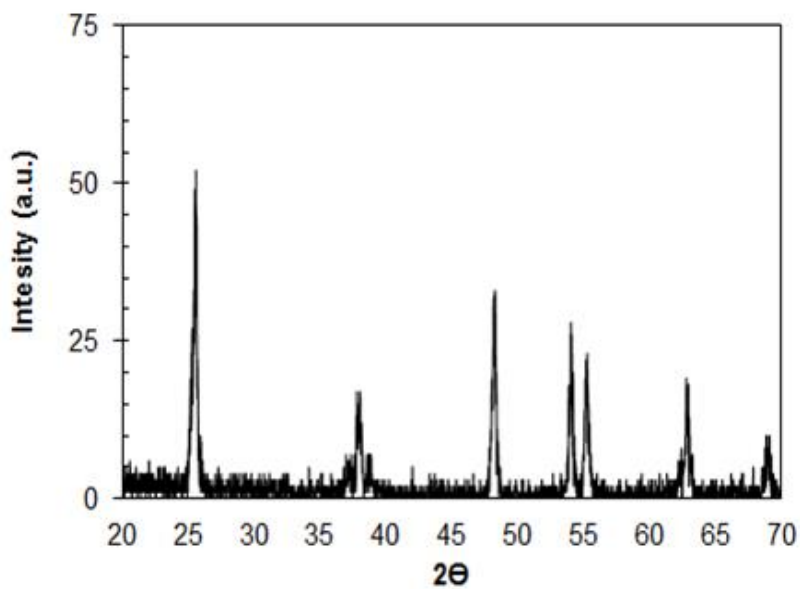


Figure 8: XRD diffractogram for two-layer glass-TiO<sub>2</sub> composite performed with water/ethanol suspension and exposed at 900°C for 4 hours of heat treatment.

## B. Particle size and polymorph phase of TiO<sub>2</sub> nanoparticles

Table 9: Size of the TiO<sub>2</sub> nanoparticles

2-Theta	$\lambda$ (nm)	FWHM	Crystallite size (nm)
25.69	0.35	0.53	16
38.23	0.24	0.55	16
38.95	0.23	0.28	37
48.48	0.19	0.61	15
54.30	0.17	0.59	16
55.50	0.17	0.67	14
63.16	0.15	0.76	13
69.11	0.14	0.58	18
70.71	0.13	0.77	13

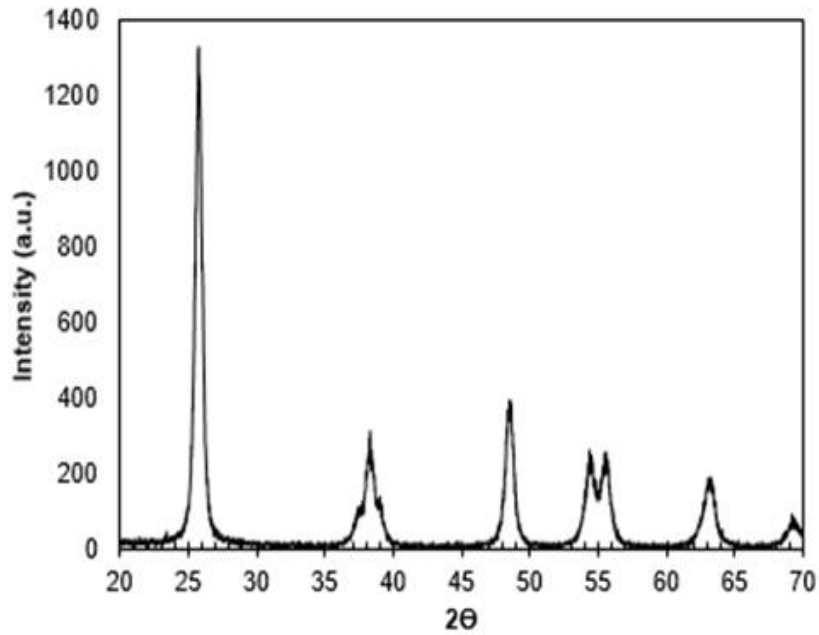


Figure 9: XRD diffractogram for two-layer glass-TiO<sub>2</sub> composite exposed at 900°C for 2 hours of heat treatment.

## Appendix C: Pseudo reaction order of atrazine degradation

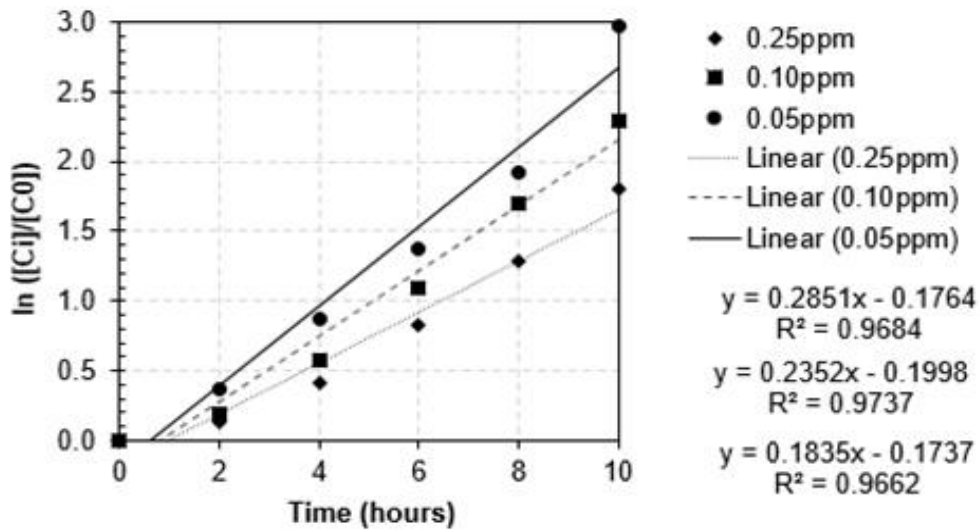


Figure 10: Reaction order of atrazine degradation with two-layer glass-TiO<sub>2</sub> composite at different concentrations of atrazine.

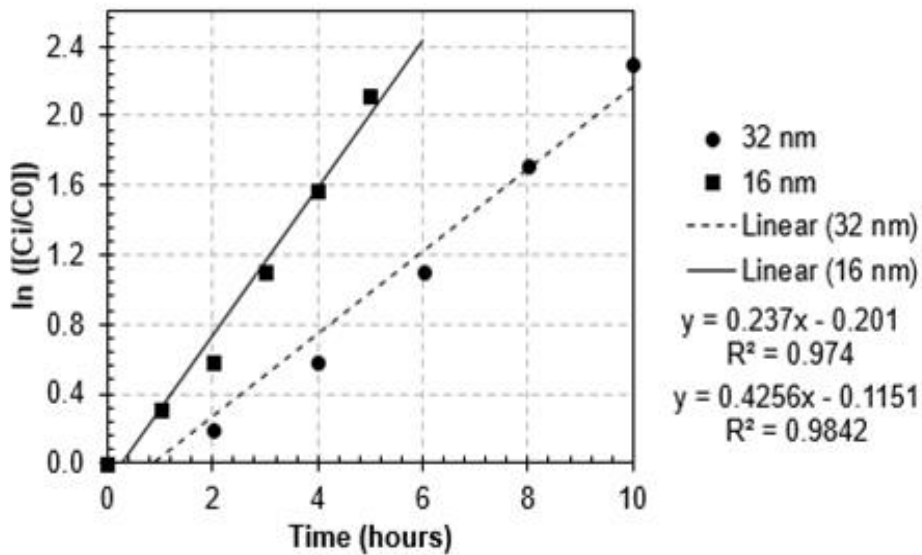


Figure 11: Reaction order of atrazine degradation with two-layer glass-TiO<sub>2</sub> composite at different particle size.